UNIVERSITY OF CALIFORNIA
RIVERSIDE

Examining California Chaparral and Coastal Sage Scrub Responses to Environmental Change: A Hydraulics Approach

A Dissertation submitted in partial satisfaction
of the requirements for the degree of

Doctor of Philosophy

in

Plant Biology

by

Alexandria Lynn Pivovaroff

June 2015

Dissertation Committee:
Dr. Louis Santiago, Chairperson
Dr. Michael Allen
Dr. David Grantz

The Dissertation of Alexandria Lynn Pivovaroff is approved:

Committee Chairperson

University of California, Riverside

Acknowledgements

The text of this dissertation, in part or in full, is a reprint of the material as it appears in Pivovaroff, A.L., Sack L., and Santiago L.S. (2014) Coordination of stem and leaf hydraulic conductance in southern California shrubs: A test of the hydraulic segmentation hypothesis. New Phytologist, 203: 842-850. The co-author Louis S. Santiago listed in that publication directed and supervised the research that forms the basis for this dissertation. The co-author Lawren Sack provided additional expertise on the evaporative flux method technique. In addition, I would like to thank my dissertation committee members Louis S. Santiago, David A. Grantz, and Michael F. Allen, and collaborators George L. Vourlitis and Sylvain Delzon. Additional support in the lab and field was provided by Pablo Pablo Bryant at the Santa Margarita Ecological Reserve and Sky Oaks Field Station, Max Brodie, Mark De Guzman, Delores Lucero, Brandon McNellis, Angelica Nunez, Sarah Pasquini, Eric Pivovaroff, Yong Shen, Victoria Woods, and Larissa Yates. Financial support was provided by a National Science Foundation Graduate Research Fellowship (NSF GRFP; DGE-1326120), a National Science Foundation Graduate Research Opportunities Worldwide Fellowship (NSF GROW), and a University of California Riverside Dissertation Year Fellowship (UCR DYP).

Dedication

This dissertation is dedicated to Eric Pivovaroff.

ABSTRACT OF THE DISSERTATION

Examining California Chaparral and Coastal Sage Scrub Responses to Environmental Change: A Hydraulics Approach

by

Alexandria Lynn Pivovaroff

Doctor of Philosophy, Graduate Program in Plant Biology
University of California, Riverside, June 2015
Dr. Louis Santiago, Chairperson

Environmental change is occurring at an unprecedented rate. Being sessile and unable to escape rapidly changing conditions, many plant species will be unable to cope with the increased abiotic stress. This may lead to decreased physiological functioning and/or mortality. Drought and nitrogen deposition are two major disturbances that affect vegetation in California's Mediterranean-type climate region. This region is a biodiversity hotspot and conservation priority. This research examined: 1) How water movement is coordinated among plant organs and the role this plays in drought adaptation; 2) The effects of long-term nitrogen deposition on plant hydraulic and drought adaptation traits; and 3) The mechanism underlying the open-vessel artifact when determining xylem vulnerability to cavitation using the centrifuge-based Cavitron. These results demonstrated that leaves act as hydraulic bottlenecks for vulnerable species, supporting the hydraulic segmentation hypothesis. In addition, *Artemisia californica* was

highly responsive to alleviation of nitrogen limitation, displaying increasing gas exchange and stem water transport, and altered functional traits. Finally, the Champagne effect was confirmed as a culprit behind the early loss of conductance in 'r' shaped vulnerability curves measured using the Cavitron. Xylem water extraction curves compared with vulnerability curves showed when true cavitation was occurring. Overall, this research shows different species have different suites of traits that result in drought adaptation, indicating that not all species will respond equally to disturbance. Additionally, proper techniques and equipment are essential to correctly quantifying these traits.

Table of Contents

List of Figures

List of Tables

Introduction

Water transport in plants is classically viewed as a passive process. Water evaporates at the leaf surface, generating tension that is transferred through the entire plant vascular system, resulting in gradients of negative pressures. The resulting transpirational pull leads to sap ascent via a continuous column of liquid from roots to shoots to leaves through xylem vessels, as described by the cohesion-tension theory (Dixon & Joly, 1895). The cohesion-tension theory explains this pulling effect and the maintenance of the metastable conditions of water in xylem conduits by cohesion between water molecules and adhesion between water molecules and xylem cell walls, both due to hydrogen bonds. The fluid dynamics within xylem reveals an incredible biophysical system. Negative pressures within xylem vessels routinely become extremely low without fatally impacting overall function. For example, *Callitris collumellaris* holds the world record for cavitation resistance, with the ability to tolerate a water of potential of -16MPa and still maintain overall plant function (Sylvain Delzon, pers. comm.).

Environmental change is increasing abiotic stress, sometimes past critical thresholds that some species cannot tolerate. For example, climate change is increasing mean global temperatures and altering precipitation regimes. Many species are already operating at the edge of their tolerance, and changes such as this are leading to mortality and loss of biodiversity. Global climate change type drought, or drought that occurs in conjunction with water temperatures due to climate change, is more extreme in intensity and duration that normal rainless periods and is already causing regional mortality events on every forested continent (Allen, 2009). Plant hydraulic failure is believed to be a

primary cause of mortality during drought. Hence, studying plant hydraulics is important for forecasting these impacts on woody plants. When the biophysical system of xylem experiences pressures or water potentials beyond its capacity, cavitation or the formation of gas emboli in xylem conduits blocks water transport. Because tensions would need to exceed 100 MPa to overcome the cohesion between water molecules to nucleate cavitation, this is not the mechanisms of embolism formation (Apfel, 1972; Pickard, 1982). Instead, drought-induced xylem cavitation is caused by air-seeding, when gas is pulled into functioning xylem vessels via intervessel pores (Zimmermann, 1983). When a xylem vessel is gas-filled it is no longer functional. If enough of the vascular system becomes compromised, other processes are diminished, including growth and photosynthesis, ultimately leading to mortality. Different species have different thresholds for tolerating very low water potentials before hydraulic failure occurs. The most common metric for comparing this threshold between species is the water potential at which 50% of hydraulic conductivity is lost (P_{50}).

P_{50} is calculated from vulnerability curves. The number of published vulnerability curves has increased exponentially in the past decade, with a notable shift in methodology (Cochard *et al*., 2013). While many curves are still generated using the 'gold standard' bench dehydration method, the majority of curves are now generated using centrifugation. There are two principle techniques for generating centrifuge-based vulnerability curves: the static-rotor method and the flow-rotor method, also known as the Cavitron (Cochard, 2002). With the static-rotor method, stems are spun in a centrifuge using a custom-built rotor to generate tensions that simulate water potentials in

the stem. Stems are removed from the centrifuge to measure hydraulic conductivity, with the spinning and removing repeated until >90% of conductivity is lost. With the Cavitron, stems are spun while water simultaneously flows through them to measure conductivity. While all centrifuge-generated vulnerability curves are constructed faster and with less plant material than bench dehydration vulnerability curves, the Cavitron eliminates the added step of removing stems from the centrifuge to measure hydraulic conductivity, allowing high-throughput. Unfortunately, all centrifuge-generated vulnerability curves may be subject to artifacts when measuring long-vesselled species (Cochard *et al*., 2005; Li *et al*., 2008; Martin-StPaul *et al*., 2014; Torres-Ruiz *et al*., 2014a).

In a recent review, John Sperry said, "Plant hydraulics provides a physically constrained bridge between the physiological regulation of transpiration and the environmental drivers of climate and hydrology" (Sperry & Love, 2015). The overall goal of this dissertation was to study drought adaptation traits, including P_{50}, in California's Mediterranean-type region, which may be a climate change hotspot. While the vegetation in this region is already adapted to surviving the annual seasonal drought, longer, more intense, more expansive, or more frequent drought brought on by climate change will be a significant threat for many species. Global climate change type drought is not the only threat, however. Other anthropogenic disturbances, including nitrogen deposition, also threaten this region. Hence, this research, which examines suites of drought adaptation traits, responses to long-term nitrogen deposition, and mechanisms behind artifacts associated with measuring P_{50}, will contribute to our understanding of this system.

References

Allen CD. **2009**. Climate-induced forest dieback: an escalating global phenomenon. *Unasylva* **231**: 60.

Apfel RR. **1972**. The Tensile Strength of Liquids. *Scientific American* **227**.

Cochard H. **2002**. A technique for measuring xylem hydraulic conductance under high negative pressures. *Plant, Cell & Environment* **25**: 815–819.

Cochard H, Badel E, Herbette S, Delzon S, Choat B, Jansen S. **2013**. Methods for measuring plant vulnerability to cavitation: a critical review. *Journal of Experimental Botany* **64**: 4779–4791.

Cochard H, Damour G, Bodet C, Tharwat I, Poirier M, Améglio T. **2005**. Evaluation of a new centrifuge technique for rapid generation of xylem vulnerability curves. *Physiologia Plantarum* **124**: 410–418.

Dixon HH, Joly J. **1895**. On the Ascent of Sap. *Philosophical Transactions of the Royal Society of London* **186**: 563–576.

Li Y, Sperry JS, Taneda H, Bush SE, Hacke UG. **2008**. Evaluation of centrifugal methods for measuring xylem cavitation in conifers, diffuse- and ring-porous angiosperms. *New Phytologist* **177**: 558–568.

Martin-StPaul NK, Longepierre D, Huc R, Delzon S, Burlett R, Joffre R, Rambal S, Cochard H. **2014**. How reliable are methods to assess xylem vulnerability to cavitation? The issue of 'open vessel' artifact in oaks. *Tree physiology*: 1–12.

Pickard WF. **1982**. The ascent of sap in plants. *Progress in Biophysics and Molecular Biology* **37**: 181–229.

Sperry JS, Love DM. **2015**. What plant hydraulics can tell us about responses to climate-change droughts. *New*.

Torres-Ruiz JM, Cochard H, Mayr S, Beikircher B, Diaz-Espejo A, Rodriguez-Dominguez CM, Badel E, Fernández JE. **2014**. Vulnerability to cavitation in Olea europaeacurrent-year shoots: further evidence of an open-vessel artefact associated with centrifuge and air-injection techniques. *Physiologia Plantarum*: n/a–n/a.

Zimmermann MH. **1983**. *Xylem structure and the ascent of sap*. Berlin: Springer-Verlag.

Chapter 1: Coordination of stem and leaf hydraulic conductance in southern California shrubs: A test of the hydraulic segmentation hypothesis

Abstract

Coordination of water movement among plant organs is important for understanding plant water use strategies. The Hydraulic Segmentation Hypothesis (HSH) proposes that hydraulic conductance in shorter-lived, 'expendable' organs such as leaves and longer-lived, more 'expensive' organs such as stems may be decoupled, with resistance in leaves acting as a bottleneck or "safety valve." We tested the HSH in woody species from a Mediterranean-type ecosystem by measuring leaf hydraulic conductance (K_{leaf}) and stem hydraulic conductivity (K_S). We also tested if leaves function as safety valves by relating K_{leaf} and hydraulic safety margin ($\Psi_{stem} - \Psi_{50}$). We also examined related plant traits including operating range of water potentials, wood density, leaf mass per area, and leaf area to sapwood area ratio to provide insight into whole plant water use strategies. For hydrated shoots, K_{leaf} was negatively correlated with K_S, supporting the HSH. Additionally, K_{leaf} was positively correlated with hydraulic safety margin and negatively correlated with leaf area to sapwood area ratio. Consistent with the HSH, our data indicate that leaves may act as control valves for species with high K_S, or low safety margin. This critical role of leaves appears to contribute importantly to plant ecological specialization in a drought prone environment.

Introduction

Hydraulic architecture refers to the arrangement of hydraulic resistances in the xylem of plants, and is a critical determinant of plant function (Zimmermann, 1978; McCulloh & Sperry, 2005). Hydraulic traits regulate the use and loss of water and influence other physiological processes, including gas exchange and growth (Zimmermann, 1978; Sperry, 2000; Santiago *et al.*, 2004a; McCulloh & Sperry, 2005; Brodribb *et al.*, 2010). The key parameter in describing hydraulic relationships is hydraulic conductance, a measure of the efficiency of water movement through a material such as plant stems or leaves (Sperry *et al.*, 1988; Choat & PrometheusWiki contributors). The definition of hydraulic conductance is based on an analogy with Ohm's law:

$$R=\Delta V/I \qquad \text{eqn. (1)}$$

where R is resistance, ΔV is the difference in voltage (potential difference), and I is current (flow of electric charge). For plant water transport, we take plant hydraulic conductance as the inverse of hydraulic resistance, pressure analogous to voltage, and flow rate analogous to current. Hence we can model plant hydraulic conductance as the flow of water for a given pressure or water potential difference:

$$k_h=F/\Delta P \qquad \text{eqn. (2)}$$

where k_h is hydraulic conductance, F is flow rate, and ΔP is pressure difference.

Evaporation at the leaf surface generates a tension or transpirational pull that is ultimately transferred throughout the plant (Tyree 1997). Water moves through plants within the soil-plant-atmosphere continuum (SPAC) as a continuous column of liquid from areas of less negative water potential to more negative water potential, as described

by the cohesion-tension theory (Dixon & Joly, 1895). However, studies have most often focused on hydraulic conductance in single plant organs, i.e., within only leaves, stems, or roots. This typical focus on individual plant organs has led to a lack of understanding of how hydraulic conductance is *coordinated* between organs such as stems and leaves. One might assume that because stems supply leaves with water, stem and leaf hydraulic conductance would increase in tandem. Conversely, discrete organs could vary in their hydraulic conductance. For example, if distal organs such as leaves had lower hydraulic conductance than large, main stems, this decoupling would maintain water status of longer-lived and more 'expensive' organs that represent a significant carbon investment at the expense of shorter-lived and 'cheaper' organs that can be more easily replaced (Zimmermann, 1983). This 'Hydraulic Segmentation' Hypothesis (HSH), as first proposed by Zimmermann, is in fact one explanation for the distribution of relative hydraulic resistance in woody plants (Tyree & Zimmermann, 2002), because greater hydraulic resistance in distal organs may function as a 'bottleneck' to water flow through the whole plant (Zimmermann, 1978; Sack & Holbrook, 2006). Early research on some diffuse-porous trees indicated that leaves and small, terminal branches represented a 'distinct hydraulic constriction' in woody plants, with lower hydraulic conductance than main stems (Zimmermann, 1978). This segmentation principle was later separated into two distinct mechanisms: *hydraulic segmentation* and *vulnerability segmentation* (Tyree & Ewers, 1991; Tyree & Zimmermann, 2002). Vulnerability segmentation refers to distal organs being more vulnerable to cavitation than basal portions, and several studies have shown that leaves tend to be more vulnerable to hydraulic decline than stems (Tyree *et*

al., 1993; Tsuda & Tyree, 1997; Choat *et al.*, 2005; Hao *et al.*, 2007; Chen *et al.*, 2009; Johnson *et al.*, 2011; Bucci *et al.*, 2012). The putative role behind segmentation, whether hydraulic or vulnerability, is the concept that "leaves function as a safety valve"(Chen *et al.*, 2009; 2010), and previous studies have demonstrated support of this "safety valve" hypothesis (Chen *et al.*, 2009; Johnson *et al.*, 2009; Chen *et al.*, 2010; Johnson *et al.*, 2011; 2012; McCulloh *et al.*, 2013), although these data generally come from relatively humid environment. The aim of this study was to test the relationship between water movement in stems and leaves in the context of the HSH in a water-limited and highly seasonal environment.

Understanding coordination of water movement between the stem and leaf may be of particular importance, especially in ecosystems with seasonal water availability. In Mediterranean-type ecosystems, plants face the dual challenge of providing water to support rapid growth during the brief wet winter and conducting water across drastically different water potential gradients during the extended dry summer (Cowling *et al.*, 2005). We first tested whether the relative resistance to water transport varied between stems and leaves, and investigated the ecological implications. We hypothesized that leaf hydraulic conductance would be negatively correlated with stem hydraulic conductivity, in support of the HSH. In addition, we tested whether leaves function in a manner similar to a "safety valve," hypothesizing species with a lower hydraulic safety margin would also have a lower leaf hydraulic conductance (Meinzer *et al.*, 2009; Delzon & Cochard, 2014). Finally, we quantified additional functional traits, including leaf mass per area, leaf area to sapwood area ratio, and wood density, along with operating stem and leaf

water potentials, to evaluate the relationships among these traits, to characterize overall plant water use strategies in the context of hydraulic segmentation, and to explore new implications for the cross-species coordination of hydraulic conductance between stems and leaves.

Materials and Methods

Study site and species

The study was conducted from 2011-2013 at the Santa Margarita Ecological Reserve (SMER; 33°29' N, 117°09' W), located at the Riverside-San Diego county line, California, USA. The reserve size is 1790 ha, with elevation ranging from 150 to 700 m. SMER has a Mediterranean-type climate and receives 36 cm of mean annual precipitation, mostly during the winter months (November – March) resulting in an annual seasonal drought between April – October. SMER has a mean annual temperature of 16.4^{o}C (Vourlitis & Pasquini, 2009) and last burned >35 years ago. This study focused on the 17 most commonly occurring woody species at SMER (Table 1), with reported maximum vessel lengths varying from 0.29 m in *Adenostoma fasciculatum* to 1.96 m in *Quercus agrifolia* (Jacobsen *et al.*, 2012). All samples were collected from the field during morning hours (0800 – 1200 h).

Water potentials

Predawn and midday water potentials (Ψ; MPa) were measured to establish seasonal variation in the water potential gradient driving flow. Measurements were taken on

bagged and un-bagged branches during the 2012 wet season (February; 15.1 cm of precipitation from November 2011 – February 2012, NOAA Fallbrook 5 and 6.5 NE CA US stations) and dry season (September; 0.5 cm of precipitation from June – September 2012, NOAA Fallbrook 5 and 6.5 NE CA US stations) with a pressure chamber (Model 1000, Plant Moisture Stress Instruments, Albany, Oregon, USA) to determine ranges of plant water status. The day prior to measurements, two branches on each of five individuals per species were covered with plastic bags and aluminum foil to stop those selected samples from transpiring and allow leaf and stem water potentials to equilibrate. Immediately following collection, branches were placed in plastic bags before being sealed and placed in a dark cooler. For predawn Ψ, one transpiring and one non-transpiring sample pair were measured from each individual. This was repeated for midday Ψ measurements. The non-transpiring Ψ measurements were taken to represent stem water potential (Ψ_{stem}) and the transpiring Ψ measurements were taken to represent leaf water potential (Ψ_{leaf}). We did not measure dry season water potentials for species that did not have leaves at the time of sampling, i.e., *Keckiella antirrhinoides*, *Mimulus aurantiacus*, *Sambucus nigra*, and *Salvia mellifera*. For each species within each season, we calculated the diurnal range in Ψ_{stem} ($\Delta\Psi_{stem}$) as the difference between midday and predawn Ψ_{stem}, and that for the leaf (Ψ_{leaf}) as the difference between midday and predawn Ψ_{leaf}. We also calculated $\Delta\Psi_{stem\text{-}leaf}$ as the difference between midday Ψ_{stem} and Ψ_{leaf}. Finally, we calculated seasonal differences in both Ψ_{stem} and Ψ_{leaf}.

Leaf hydraulic conductance

Leaf hydraulic conductance (K_{leaf}) was measured during the spring (March-June) on newly mature leaves from at least four individuals of each species, using the evaporative flux method (Sack *et al.*, 2002; Sack & Scoffoni, 2013). In the lab, leaves from the same branches that were used for stem hydraulic conductivity (see below) were cut from the stem under water with a fresh razor blade. Leaves were immediately placed in beakers with filtered (0.2 μm), degassed water that covered the petiole, but did not touch the lamina. Samples were covered with plastic and allowed to hydrate overnight for approximately 8 hours.

Following rehydration, leaves were connected to tubing containing filtered (0.2 μm), degassed water that ran from a reservoir on a balance (±0.1 mg; Denver Instrument P-214, Sartorius, Bohemia, NY, USA) to the leaf. Leaves were held in place with a wood frame strung with fishing line, and placed over a fan to reduce the boundary layer around the leaf. Lights arranged above the sample diffused through a plexiglass container with water that acted as a heat trap and produced a photon flux density of >1200 μmol m^{-2} s^{-1} at the leaf level to induce stomatal opening.

The transpiration-driven flow of water into the leaf was measured from the balance interfaced to a computer, logging data every 60 seconds. Transpirational flow increased for ~30 minutes in the beginning of the measurement before steady-state transpiration was achieved (coefficient of variance <5%) for 10 minutes. Leaves were then placed in a Whirlpak bag and rapidly removed from the tubing to measure leaf water potential with a pressure chamber (Model 1000, Plant Moisture Stress Instruments).

Finally, leaf area was measured with a leaf area meter (LI-3100, Li-Cor Biosciences, Lincoln, Nebraska, USA). The leaf hydraulic conductance (K_{leaf}; mmol m^{-2} s^{-1} MPa^{-1}) was calculated as:

$$K_{leaf} = E/\Delta\Psi_{leaf} \qquad \text{eqn. (6)},$$

normalized by leaf area (m^2), where E is the steady-state transpiration flow rate (mmol s^{-1}) and $\Delta\Psi_{leaf}$ is the water potential driving force ($-\Psi_{leaf}$; MPa).

Stem hydraulic conductivity and xylem vulnerability

Large branch samples approximately 1 m in length were collected from at least four individuals of each species in the field. Cut ends were covered with parafilm and samples were placed in opaque plastic bags with wet paper towels until transported to the lab. Once in the lab, stem samples were cut under water to a length of approximately 16 cm. Emboli were removed from stems by vacuum infiltration under filtered (0.2 μm) water for 8 hrs. Stem ends were then re-cut under water and ends cleanly shaven with a razor blade for a final sample length of 14.2 cm.

Maximum stem hydraulic conductivity (K_{max}) was determined by connecting stems to tubing filled with filtered (0.2 μm), de-gassed water flowing from an elevated source, through the stem, and into a reservoir on a balance (±0.1 mg; Denver Instrument P-214, Sartorius, Bohemia, NY, USA) that was interfaced with a computer to record the flow rate, allowing the calculation of conductivity (Sperry *et al.*, 1988). Following Torres-Ruiz *et al.*, (2012), we corrected for stem passive water uptake by beginning and ending each conductivity measurement with a 'background' measurement. Stem hydraulic

conductivity (K_h; kg m s^{-1} MPa^{-1}) was calculated as:

$$K_h = F \times L / \Delta P \qquad \text{eqn. (3)},$$

where F is the flow rate (kg s^{-1}), L is the stem length (m), and ΔP is the driving force (MPa). Stem hydraulic conductivity was also normalized by sapwood area (A_{SW}; m^2) to determine stem sapwood-specific hydraulic conductivity (K_S; kg m^{-1} s^{-1} MPa^{-1}), and distal leaf area (A_L; m^2) to determine leaf specific hydraulic conductivity (K_L; kg m^{-1} s^{-1} MPa^{-1}).

Stem xylem vulnerability to cavitation, as determined by vulnerability curves, was measured using the 'static' centrifugation method (Alder *et al.*, 1997; Sperry *et al.*, 2012; Jacobsen & Pratt, 2012) to determine the water potential at which 50% of conductivity is lost (Ψ_{50}) and calculate the stem hydraulic safety margin (Meinzer *et al.*, 2009; Delzon & Cochard, 2014). The static centrifugation method differs from the cavitron, or flow centrifugation, method in that hydraulic conductivity is measured between spinning, whereas conductivity is measured during spinning with the cavitron (Cochard *et al.*, 2005).

Following the determination of maximum K_h (K_{max}), stems were spun using a custom built, 14.2 cm diameter rotor in a refrigerated centrifuge (Sorvall RC-5Cplus, Thermo Scientific, Waltham, MA, USA) at progressively more negative stem water potentials to cause embolisms. Foam cosmetic sponges soaked with water were added to the vertical end of the plexiglass reservoirs to keep the ends of the stems wet, even when the rotor was not spinning (Jacobsen & Pratt, 2012; Tobin *et al.*, 2012). ΔP was always kept below 2 kPa to prevent possible flushing of embolisms induced by centrifugation in wide and/or open vessels. Hydraulic conductivity was repeatedly measured on each stem

after spinning at increasing speeds, and K_h declined with more negative water potentials and increasing levels of xylem cavitation. This was repeated until the stem lost >90% conductivity. Percent loss of conductivity (PLC) was calculated at each water potential step as:

$$PLC = 100\times(1-(K_h/K_{max}) \quad \text{eqn. (4).}$$

Vulnerability curves were constructed by plotting water potential versus PLC and fitting a Weibull model (Pammenter & Willigen, 1998):

$$PLC = 100/(1+\exp(a(\Psi-b))) \quad \text{eqn. (5)}$$

from which stem Ψ_{50} was determined for each species. Stem hydraulic safety margin as calculated as midday $\Psi_{stem} - \Psi_{50}$ (Meinzer *et al.*, 2009; Delzon & Cochard, 2014).

Functional traits: Leaf area to sapwood area ratio, leaf mass per area, and wood density

Branch level measurements of leaf area to sapwood area ratio (LA:SA) were made during the spring (March-June) to determine the relationship between total transpiring leaf area and the area of sapwood supplying water to those leaves (Shinozaki *et al.*, 1964; Martínez-Vilalta & PrometheusWiki contributors). Cross-sectional sapwood area of excised branch samples was determined by removing bark and measuring the diameter of the sapwood with digital calipers to calculate the cross-sectional area. If pith was present, its cross-sectional area was subtracted from total sapwood area. All distal leaves were removed from the stem segment, and their total area was measured using a leaf area meter (LI-3100, Li-Cor Biosciences).

Leaf mass per area (LMA), was determined for individual leaves by measuring leaf

area using a leaf area meter (LI-3100), drying leaves for 48h at 65°C before measuring dry mass, and dividing dry mass (g) by fresh leaf area (m^2).

Wood density was measured by removing the bark and pith from stem sub-samples and determining the fresh volume with the water displacement method (Williamson & Wiemann, 2010; Osazuwa-Peters *et al.*), then drying the xylem for 48h at 65°C before measuring dry mass. Woody density (g cm^{-3}) was calculated as the ratio of xylem dry mass (g) to fresh volume (cm^3).

Statistics

We used Pearson's product-moment correlation coefficients to evaluate interspecific bi-variate relationships among physiological variables using SAS Software ver. 9.3 (SAS Institute, Inc., Cary, NC, USA). Before testing correlations, when trait values were not normally distributed, they were $\log_{10}$-transformed, which resulted in normal distributions. Negative values were converted to positive values to enable $\log_{10}$-transformation when necessary (e.g., Ψ). The overall difference between $\Delta\Psi_{stem}$ and $\Delta\Psi_{leaf}$ was analyzed using paired *t*-test. *Rhamnus ilicifolia* Ψ_{50} was removed from hydraulic safety margin analyses because its calculated Ψ_{50} was beyond the range of collected data. We also evaluated the impact of phylogenetic relationships for our analyzed trade-offs using phylogenetically independent contrasts (PICs) with the R "ape" package (ver. 3.0-11) (Paradis *et al.*, 2004). Phylomatic (ver. 3) was used to build the tree and Phylocom (ver. 4.2) to add branch lengths (Webb *et al.*, 2008).

Results

Measurement of Ψ_{leaf} and Ψ_{stem} indicated that the study species experienced a wide range of tissue water status on an annual basis (Figure 1). Midday Ψ_{leaf} (Figure 1c) ranged from -1.19 MPa in *Schinus molle* during the wet season to -9.39 MPa in *Olea europaea* during the dry season. Midday Ψ_{stem} (Figure 1d) ranged from a maximum of -0.95 MPa in *Schinus molle* during the wet season to a minimum of -8.66 MPa in *Xylococcus bicolor* during the dry season. Seasonal differences (Figure 1) of midday Ψ between the wet and dry season also varied, with *Malosma laurina* exhibiting the smallest difference at 0.05 MPa for leaves and 0.15 MPa for stems and *X. bicolor* exhibiting the largest difference at 6.64 MPa for leaves and 7.08 MPa for stems. The diurnal range in Ψ_{leaf} ($\Delta\Psi_{leaf}$) was always greater in magnitude than that of the stem ($\Delta\Psi_{stem}$) for both the wet (P<0.0001) and dry season (P=0.0025) (Figure 2). $\Delta\Psi_{stem\text{-}leaf}$ was not correlated with any measured traits.

Values for K_{leaf} were negatively correlated with K_S (r= -0.54, P=0.02; PIC r= -0.51, P=0.04; Figure 3), with species having greater K_S exhibiting lower K_{leaf}, supporting the HSH. Operating hydraulic safety margin (February midday Ψ_{stem} – stem Ψ_{50}) and K_{leaf} were positively correlated (Figure 4), with species having stems that operate within a smaller safety margin also having lower K_{leaf}, consistent with leaves acting as a safety valve. We also found a negative relationship between K_{leaf} and LA:SA (r= -0.56, P=0.02; PIC r= -0.66, P=0.004; Figure 5a) and a positive relationship between K_S and LA:SA (r=0.62, P=0.008; Figure 5b). Additional significant relationships include K_S and stem Ψ_{50} as negatively related (r= -0.48, P=0.06; PIC r=-0.61 P=0.009) and K_{leaf} and stem Ψ_{50}

(-MPa) as positively related (r=0.52, P=0.04; PIC r=0.55 P=0.02). K_L was not correlated with any other measured traits.

There was a positive correlation between LMA and wood density (r=0.66, P=0.004; PIC r=0.66 P=0.003; Figure 6). LMA was negatively correlated with wet season predawn Ψ_{stem} and Ψ_{leaf} (r= -0.65, P=0.005, and r= -0.58, P=0.01, respectively) and midday Ψ_{stem} (r= -0.56, P=0.02; Table 2), but not with any dry season Ψ measurements. Wood density was negatively correlated with wet season predawn and midday Ψ_{stem} (r= -0.70, P=0.002, and r= -0.61, P=0.009, respectively) and Ψ_{leaf} (r= -0.71, P=0.001, and r=-0.58, P=0.01, respectively), and dry season midday Ψ_{stem} (r= -0.60, P=0.03; Table 2), but not with dry season predawn Ψ_{stem} or Ψ_{leaf}, or midday Ψ_{leaf}.

Discussion

We found a negative relationship between K_S and K_{leaf} (Figure 3), indicating that for woody shrubs in the California Mediterranean-type ecosystem, species with higher stem conductivity rely on low leaf hydraulic conductance to place limits on water loss during maximum gas exchange and thus act to maintain water status of basal organs at the expense of distal organs. The role of leaves as safety valves was further clarified by the positive relationship between hydraulic safety margin and K_{leaf} (Figure 4), as species with stems that operate in a more narrow safety range may rely on hydraulic resistance in the leaves to act as a bottleneck to water flow, whereas species that operate within a wider safety range have higher K_{leaf} consistent with less need of protection. Thus, the resistance to water transport at the leaf level has the potential to protect longer-lived and more

costly woody stems farther down the soil-plant-atmosphere continuum from reaching critical xylem water potentials that could produce catastrophic hydraulic failure, as hypothesized by Zimmermann (1983) in the original formulation of the HSH.

The inverse arrangement of hydraulic conductances of stems and leaves was related to shoot allometry. We found a negative relationship between K_{leaf} and LA:SA (Figure 5a), demonstrating a balance between water movement in individual leaves and overall shoot transpirational demand. Plants with overall more leaf area for a given sapwood area exhibited lower maximum K_{leaf} on an individual leaf area basis, while conversely species with lower LA:SA had higher K_{leaf} as there was relatively less leaf area on a shoot competing for water from the transpirational stream. This finding is consistent with our sampling across species within a community that are subject to approximately the same precipitation and water availability. The negative relationship points to a constraint on total leaf area by the capacity of stems to support leaf water loss among these co-existing species. In contrast, a previous study of six *Nothofagus* species along five sites spanning a precipitation and elevation gradient reported a positive correlation between K_{leaf} and LA:SA (Bucci *et al.*, 2012). Yet, the *Nothofagus* system receives up to more than four times the precipitation of the current study and is arranged along an altitudinal gradient, suggesting that altitudinal constraints limit both LA:SA and K_{leaf}. We also found a positive relationship between K_S and LA:SA (Figure 5b), as previously reported for different species sets (Choat *et al.*, 2011; Gleason *et al.*, 2012). The LA:SA is a major determinant of plant hydraulic architecture (Martínez-Vilalta & PrometheusWiki contributors), consistent with the pipe model theory (Shinozaki *et al.*,

1964), and previous studies have shown similar cases of balancing transpiring leaf area with stem conductive supply through the plant (Meinzer & Grantz, 1990).

Our results indicate large variation in plant water use strategies among co-occurring species. This pattern indicates that withstanding drought in this semi-arid Mediterranean-type climate can be accomplished by adjustment in multiple traits. For example, *S. mellifera* and *K. antirrhinoides* are both deciduous species that drop their leaves during the dry season and physiologically "shut down." While they both "avoid" drought through deciduous leaf phenology, they operate within different safety margins, with *K. antirrhinoides* having a much larger safety margin than *S. mellifera* (Figure 4*)*. Similarly, *M. laurina* and *X. bicolor* are both evergreen species that "tolerate" drought by holding onto their leaves and continuing to function during the dry season, but *X. bicolor* operates in a much larger safety margin than *M. laurina* (Figure 4). As such, our data are consistent with coordination of multiple traits, including water acquisition, stomatal control of water loss, and resistance to cavitation, to maintain hydraulic function (Meinzer & Grantz, 1991; Santiago *et al.*, 2004b; Meinzer *et al.*, 2009; Jones *et al.*, 2010). Thus, species with similarity in one trait can have large variation in other traits, allowing for complex combinations of hydraulic strategy variation that may promote species coexistence at this site (Wright, 2002; Sack *et al.*, 2005; Marks & Lechowicz, 2006; Angert *et al.*, 2009). Additionally, new attention has been called to the hydraulic safety margin of woody plants (Delzon & Cochard, 2014), with differences in species' susceptibility to mortality found to be related to differences in their hydraulic safety margins (Plaut *et al.*, 2012), though drought-induced tree mortality is a complex process

with multiple interacting factors (McDowell *et al.*, 2008; Anderegg *et al.*, 2012). These differences in hydraulic safety margin for co-occurring species at our site may have implications for shifts in community structure under climate change.

As xylem pressure is the driving force behind hydraulic conductance as explained by Ohm's law (Tyree 1997), we also examined how water status and water transport capacity were related to LMA and wood density. LMA and wood density are relatively easy-to-measure functional traits that offer a potentially rapid way to characterize physiological tendencies for many species. Yet how well these traits perform for predicting physiological processes for a particular species varies greatly across sites and species (Wright *et al.*, 2006). Species with high LMA tend to exhibit longer leaf lifespans, relatively low leaf nitrogen concentration, and low maximum photosynthetic rates (Wright *et al.*, 2004), whereas species with high wood density tend to exhibit low maximum hydraulic conductivity (Santiago *et al.*, 2004b) and greater stem xylem resistance to cavitation (Hacke *et al.*, 2001; Delzon *et al.*, 2010). Therefore, our data indicating that LMA and wood density were correlated with each other (Figure 6) and with various measures of water stress (Table 2) are consistent with previous findings in the literature (Wright *et al.*, 2006; Westoby & Wright, 2006). Species with higher wood density had higher LMA, showing greater investment in structure of stems and leaves, while species with lower wood density had lower LMA, possibly to maximize resource acquisition at the cost of safe structure. Overall, wood density and LMA were more correlated with wet season than dry season measures of water potential (Table 2), suggesting that wood density and LMA are optimized for resource capture during

seasonally brief environmentally favorable conditions. Furthermore, species with more negative wet season water potentials also had greater wood density (Table 2), which is consistent with previous findings implicating wood density in drought tolerance (Hacke *et al.*, 2001; Delzon *et al.*, 2010; Bucci *et al.*, 2012).

Our result of a negative correlation between water transport in stems and leaves, which supports the HSH, has important implications for plant hydraulic strategies. Suites of traits, including resistance to cavitation, leaf phenology, and rooting depth (Hellmers *et al.*, 1955; Ackerly, 2004) promote tolerance of periods of low water availability, whether on a seasonal basis or during prolonged events. Our findings highlight the role of leaf hydraulics in overall plant drought adaptation. This is especially important in the wake of environmental change, with warmer temperatures leading to global change-type drought and vegetation dieback (Allen, 2009). It should be mentioned that while we measured *maximum* stem and leaf hydraulic conductance, which may not represent performance achieved in the field, especially as plant water supply declines, such maximum capacity measurements generally scale with integrated exposure to stress and resource availability (Field, 1991). Studying how stem and leaf hydraulic conductivity vary *in vivo* diurnally and seasonally would provide additional understanding of coordination of hydraulic and functional traits, as well as plant ecological strategy variation with respect to balancing water use to maximize growth and maintenance of water potential in the face of seasonal water deficit. Future studies may focus on additional plant growth forms and biomes to address the ecosystem dependency of established site-based patterns (Reich, 1993).

References

Ackerly DD. **2004**. Functional strategies of chaparral shrubs in relation to seasonal water deficit and disturbance. *Ecological Monographs* **74**: 25–44.

Alder N, Pockman WT, Sperry JS, Nuismer S. **1997**. Use of centrifugal force in the study of xylem cavitation. *Journal of Experimental Botany* **48**: 665–674.

Allen CD. **2009**. Climate-induced forest dieback: an escalating global phenomenon. *Unasylva* **231**: 60.

Anderegg WRL, Berry JA, Smirth DD, Sperry JS, Anderegg LDL, Field CB. **2012**. The roles of hydraulic and carbon stress in a widespread climate-induced forest die-off. *Proceedings of the National Academy of Sciences* **109**: 233–237.

Angert AL, Huxman TE, Chesson P, Venable DL. **2009**. Functional tradeoffs determine species coexistence via the storage effect. *Proceedings of the National Academy of Sciences* **106**: 11641–11645.

Brodribb TJ, Bowman DJMS, Nichols S, Delzon S, Burlett R. **2010**. Xylem function and growth rate interact to determine recovery rates after exposure to extreme water deficit. *New Phytologist* **188**: 533–542.

Bucci SJ, Scholz FG, Campanello PI, Montti L, Jimenez-Castillo M, Rockwell FA, Manna LL, Guerra P, Bernal PL, Troncoso O, *et al.* 2012. Hydraulic differences along the water transport system of South American Nothofagus species: do leaves protect the stem functionality? *Tree Physiology* **32**: 880-893.

Chen J-W, Zhang Q, Li X-S, Cao K-F. **2009**. Independence of stem and leaf hydraulic traits in six Euphorbiaceae tree species with contrasting leaf phenology. *Planta* **230**: 459–468.

Chen J-W, Zhang Q, Li X-S, Cao K-F. **2010**. Gas exchange and hydraulics in seedlings of Hevea brasiliensis during water stress and recovery. *Tree Physiology* **30**: 876–885.

Choat B, PrometheusWiki contributors. Hydraulic conductance and conductivity. *PrometheusWiki*. Accessed: 3 May 2011.

Choat B, Lahr EC, Melcher PJ, Zwieniecki MA, Holbrook NM. **2005**. The spatial pattern of air seeding thresholds in mature sugar maple trees. *Plant, Cell & Environment* **28**: 1082–1089.

Choat B, Medek DE, Stuart SA, Pasquet-Kok J, Egerton JJG, Salari H, Sack L, Ball MC. **2011**. Xylem traits mediate a trade-off between resistance to freeze-thaw-induced embolism and photosynthetic capacity in overwintering evergreens. *New Phytologist* **191**:

996–1005.

Cochard H, Damour G, Bodet C, Tharwat I, Poirier M, Améglio T. **2005**. Evaluation of a new centrifuge technique for rapid generation of xylem vulnerability curves. *Physiologia Plantarum* **124**: 410–418.

Cowling RM, Ojeda F, Lamont BB, Rundel PW, Lechmere-Oertel R. **2005**. Rainfall reliability, a neglected factor in explaining convergence and divergence of plant traits in fire-prone mediterranean-climate ecosystems. *Global Ecology and Biogeography* **14**: 509–519.

Delzon S, Cochard H. **2014**. Recent advances in tree hydraulics highlight the ecological significance of the hydraulic safety margin. *New Phytologist*: 1–4.

Delzon S, Douthe C, Sala A, Cochard H. **2010**. Mechanism of water-stress induced cavitation in conifers: bordered pit structure and function support the hypothesis of seal capillary-seeding. *Plant, Cell & Environment* **33**: 2101–2111.

Dixon HH, Joly J. **1895**. On the Ascent of Sap. *Philosophical Transactions of the Royal Society of London* **186**: 563–576.

Field CB. **1991**. Ecological scaling of carbon gain to stress and resource availability.Mooney H, Winner WE, Pell EJ eds. Response of Plants to Multiple Stresses. New York: Academic Press, 35–65.

Gleason SM, Butler DW, Ziemińska K, Waryszak P, Westoby M. **2012**. Stem xylem conductivity is key to plant water balance across Australian angiosperm species. *Functional Ecology* **26**: 343-352.

Hacke UG, Sperry JS, Pockman WT, Davis SD, McCulloh KA. **2001**. Trends in wood density and structure are linked to prevention of xylem implosion by negative pressure. *Oecologia* **126**: 457–461.

Hao G-Y, Hoffmann WA, Scholz FG, Bucci SJ, Meinzer FC, Franco AC, Cao K-F, Goldstein G. **2007**. Stem and leaf hydraulics of congeneric tree species from adjacent tropical savanna and forest ecosystems. *Oecologia* **155**: 405–415.

Hellmers H, Horton JS, Juhren G, O'Keefe J. **1955**. Root Systems of Some Chaparral Plants in Southern California. *Ecology* **36**: 667–678.

Jacobsen AL, Pratt RB. **2012**. No evidence for an open vessel effect in centrifuge-based vulnerability curves of a long-vesselled liana (Vitis vinifera). *New Phytologist* **194**: 982–990.

Jacobsen AL, Pratt RB, Tobin MF, Hacke UG, Ewers FW. **2012**. A global analysis of

xylem vessel length in woody plants. *American Journal of Botany* **99**: 1583–1591.

Johnson DM, McCulloh KA, Meinzer FC, Woodruff DR, Eissenstat DM. **2011**. Hydraulic patterns and safety margins, from stem to stomata, in three eastern US tree species. *Tree Physiology* **31**: 659–668.

Johnson DM, McCulloh KA, Woodruff DR, Meinzer FC. **2012**. Hydraulic safety margins and embolism reversal in stems and leaves: why are conifers and angiosperms so different? *Plant science : an international journal of experimental plant biology* **195**: 48–53.

Johnson DM, Woodruff DR, McCulloh KA, Meinzer FC. **2009**. Leaf hydraulic conductance, measured in situ, declines and recovers daily: leaf hydraulics, water potential and stomatal conductance in four temperate and three tropical tree species. *Tree Physiology* **29**: 879–887.

Jones TJ, Luton CD, Santiago LS, Goldstein G. **2010**. Hydraulic constraints on photosynthesis in subtropical evergreen broad leaf forest and pine woodland trees of the Florida Everglades. *Trees* **24**: 471–478.

Marks CO, Lechowicz MJ. **2006**. Alternative designs and the evolution of functional diversity. *The American naturalist* **167**: 55–66.

Martínez-Vilalta J, PrometheusWiki contributors. Water balance traits - leaf to sapwood area ratio. *PrometheusWiki*. Accessed: 3 May 2011.

McCulloh KA, Sperry JS. **2005**. Patterns in hydraulic architecture and their implications for transport efficiency. *Tree Physiology* **25**: 257–267.

McCulloh KA, Johnson DM, Meinzer FC, Woodruff DR. **2013**. The dynamic pipeline: hydraulic capacitance and xylem hydraulic safety in four tall conifer species. *Plant, Cell & Environment*.

McDowell NG, Pockman WT, Allen CD, Breshears DD, Cobb NS, Kolb T, Plaut JA, Sperry JS, West AG, Williams DG, *et al.* 2008. Mechanisms of plant survival and mortality during drought: why do some plants survive while others succumb to drought? *New Phytol.* **178**: 719–739.

Meinzer FC, Grantz DA. **1990**. Stomatal and hydraulic conductance in growing sugarcane: stomatal adjustment to water transport capacity*. *Plant, Cell & Environment* **13**: 383–388.

Meinzer FC, Grantz DA. **1991**. Coordination of stomatal, hydraulic, and canopy boundary layer properties: do stomata balance conductances by measuring transpiration? *Physiologia Plantarum* **83**: 324–329.

Meinzer FC, Johnson DM, Lachenbruch B, McCulloh KA, Woodruff DR. **2009**. Xylem hydraulic safety margins in woody plants: coordination of stomatal control of xylem tension with hydraulic capacitance. *Functional Ecology* **23**: 922–930.

Osazuwa-Peters O, Zanne AE, PrometheusWiki contributors. Wood density. *PrometheusWiki*. Accessed: 30 November 2012.

Pammenter N, Willigen C. **1998**. A mathematical and statistical analysis of the curves illustrating vulnerability of xylem to cavitation. *Tree Physiology* **18**: 589–593.

Paradis E, Claude J, Strimmer K. **2004**. APE: Analyses of Phylogenetics and Evolution in R language. *Bioinformatics* **20**: 289–290.

Plaut JA, Yepez EA, HILL J, Pangle R, Sperry JS, Pockman WT, McDowell NG. **2012**. Hydraulic limits preceding mortality in a piñon-juniper woodland under experimental drought. *Plant, Cell & Environment* **35**: 1601–1617.

Sack L, Holbrook NM. **2006**. LEAF HYDRAULICS. *Annu. Rev. Plant Biol.* **57**: 361–381.

Sack L, Scoffoni C. **2013**. Measurement of leaf hydraulic conductance and stomatal conductance and their responses to irradiance and dehydration using the Evaporative Flux Method (EFM). *Journal of visualized experiments* **70**: e4179.

Sack L, Melcher PJ, Zwieniecki MA, Holbrook NM. **2002**. The hydraulic conductance of the angiosperm leaf lamina: a comparison of three measurement methods. *Journal of Experimental Botany* **53**: 2177–2184.

Sack L, Tyree MT, Holbrook NM. **2005**. Leaf hydraulic architecture correlates with regeneration irradiance in tropical rainforest trees. *New Phytologist* **167**: 403–413.

Santiago LS, Goldstein G, Meinzer FC, Fisher JB, Machado K, Woodruff DR, Jones TJ. **2004a**. Leaf photosynthetic traits scale with hydraulic conductivity and wood density in Panamanian forest canopy trees. *Oecologia* **140**: 543–550.

Santiago LS, Kitajima K, Wright SJ, Mulkey SS. **2004b**. Coordinated changes in photosynthesis, water relations and leaf nutritional traits of canopy trees along a precipitation gradient in lowland tropical forest. *Oecologia* **139**: 495–502.

Shinozaki K, Yoda K, Hozumi K, Kira T. **1964**. A quantitative analysis of plant form - The pipe model theory. *Japanese Journal of Ecology* **14**: 97–105.

Sperry JS. **2000**. Hydraulic constraints on plant gas exchange. *Agricultural and Forest Meteorology* **104**: 13–23.

Sperry JS, Christman MA, Torres-Ruiz JM, Taneda H, Smirth DD. **2012**.

Vulnerability curves by centrifugation: is there an open vessel artifact, and are 'r' shaped curves necessarily invalid? *Plant, Cell & Environment* **35**: 601–610.

Sperry JS, Donnelly J, Tyree MT. **1988**. A method for measuring hydraulic conductivity and embolism in xylem. *Plant, Cell & Environment* **11**: 35–40.

Tobin MF, Pratt RB, Jacobsen AL, De Guzman ME. **2012**. Xylem vulnerability to cavitation can be accurately characterised in species with long vessels using a centrifuge method. *Plant Biology* **15**: 496–504.

Torres-Ruiz JM, Sperry JS, Fernández JE. **2012**. Improving xylem hydraulic conductivity measurements by correcting the error caused by passive water uptake. *Physiologia Plantarum* **146**: 129–135.

Tsuda M, Tyree MT. **1997**. Whole-plant hydraulic resistance and vulnerability segmentation in *Acer saccharinum*. *Tree Physiology* **17**: 351–357.

Tyree MT, Ewers FW. **1991**. The Hydraulic Architecture of Trees and Other Woody Plants. *New Phytologist* **119**: 345–360.

Tyree MT. 1997. The Cohesion-Tension theory of sap ascent: current controversies. *Journal of Experimental Botany 48*: 1753–1765.

Tyree MT, Zimmermann MH. **2002**. *Xylem Structure and the Ascent of Sap*. Springer.

Tyree MT, Cochard H, Cruiziat P, Sinclair B, Ameglio T. **1993**. Drought-induced leaf shedding in walnut: evidence for vulnerability segmentation. *Plant, Cell & Environment* **16**: 879–882.

Vourlitis GL, Pasquini SC. **2009**. Experimental dry-season N deposition alters species composition in southern Californian mediterranean-type shrublands. *Ecology* **90**: 2183–2189.

Webb CO, Ackerly DD, Kembel SW. **2008**. Phylocom: software for the analysis of phylogenetic community structure and trait evolution. *Bioinformatics* **24**: 2098.

Westoby M, Wright IJ. **2006**. Land-plant ecology on the basis of functional traits. *Trends in Ecology & Evolution* **21**: 261–268.

Williamson GB, Wiemann MC. **2010**. Measuring wood specific gravity…Correctly. *American Journal of Botany* **97**: 519–524.

Wright IJ, Falster DS, Pickup M, Westoby M. **2006**. Cross‐species patterns in the coordination between leaf and stem traits, and their implications for plant hydraulics. *Physiologia Plantarum* **127**: 445–456.

Wright IJ, Reich PB, Westoby M, Ackerly DD, Baruch Z, Bongers F, Cavender-Bares J, Chapin T, Cornelissen JHC, Diemer M, *et al.* 2004. The worldwide leaf economics spectrum. *Nature* **428**: 821–827.

Wright SJ. **2002**. Plant diversity in tropical forests: a review of mechanisms of species coexistence. *Oecologia* **130**: 1–14.

Zimmermann MH. **1978**. Hydraulic architecture of some diffuse-porous trees. *Canadian Journal of Botany* **56**: 2286–2295.

Zimmermann MH. **1983**. *Xylem structure and the ascent of sap*. Berlin: Springer-Verlag.

Table 1.1. Dominant woody study species, with symbols used to represent species in figures and native or non-native (NN) designation, at Santa Margarita Ecological Reserve, California, USA.

Species	Family	Symbol	Native or NN
Adenostoma fasciculatum	Rosaceae		Native
Ceanothus tomentosus	Rhamnaceae		Native
Heteromeles arbutifolia	Rosaceae		Native
Keckiella antirrhinoides	Plantaginaceae		Native
Malosma laurina	Anacardiaceae		Native
Mimulus aurantiacus	Phrymaceae		Native
Nicotiana glauca	Solanaceae		NN
Olea europaea	Oleaceae		NN
Quercus agrifolia	Fagaceae		Native
Quercus berberidifolia	Fagaceae		Native
Rhamnus ilicifolia	Rhamnaceae		Native
Rhus ovata	Anacardiaceae		Native
Sambucus nigra	Adoxaceae		Native
Salvia mellifera	Lamiaceae		Native
Schinus molle	Anacardiaceae		NN
Senna artemisioides	Fabaceae		NN
Xylococcus bicolor	Ericaceae		Native

Table 1.2. Pearson's correlation coefficients between functional traits, including leaf area to sapwood area ratio (LA:SA), wood density, and leaf mass per area (LMA), with measures of leaf and stem water potential (Ψ_{leaf} and Ψ_{stem}, respectively) for all dominant woody species growing at Santa Margarita Ecological Reserve, California, USA.

Trait	LA:SA (m^2 m^{-2})	Wood density (g cm^{-3})	LMA (g cm^{-2})
Wet season			
Predawn Ψ_{leaf} (MPa)	r=0.48, P=0.05	r= -0.71, P=0.001	r= -0.58, P=0.01
Predawn Ψ_{stem} (MPa)	.	r= -0.70, P=0.002	r= -0.65, P=0.005
Midday Ψ_{leaf} (MPa)	.	r= -0.58, P=0.01	.
Midday Ψ_{stem} (MPa)	.	r= -0.61, P=0.009	r= -0.56, P=0.02
Dry season			
Predawn Ψ_{leaf} (MPa)	.	.	.
Predawn Ψ_{stem} (MPa)	.	.	.
Midday Ψ_{leaf} (MPa)	.	.	.
Midday Ψ_{stem} (MPa)	.	r= -0.60, P=0.03	.

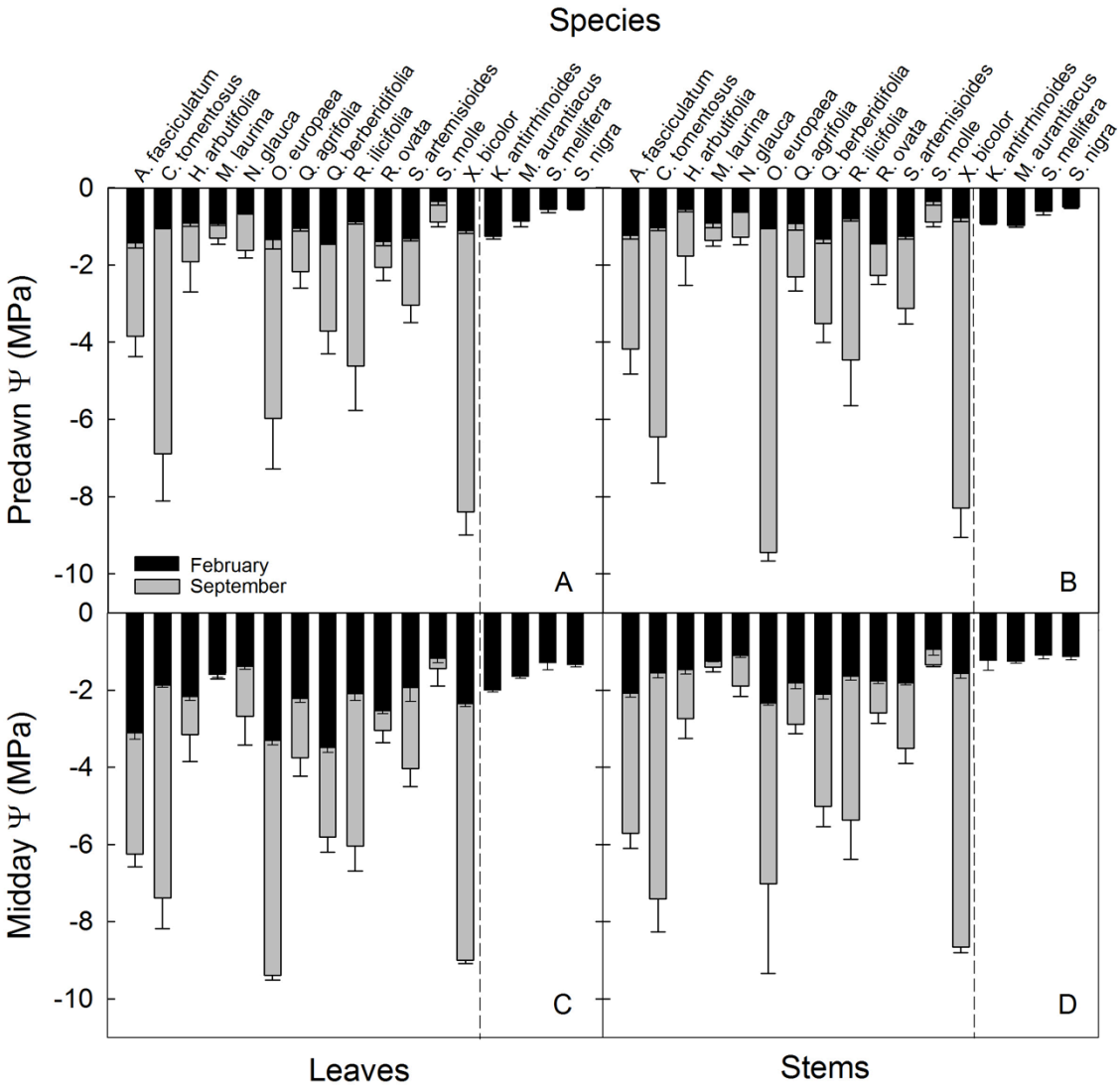

Figure 1.1. Predawn and midday stem and leaf water potentials (Ψ) measured for dominant woody species in a California Mediterranean-type climate region during the wet (February; black bars) and dry (September; grey bars) season. Panels: (a) predawn Ψ_{leaf}; (b) predawn Ψ_{stem}; (c) midday Ψ_{leaf}; (d) midday Ψ_{stem}. Water potentials were not measured on deciduous species during the dry season as they had no leaves.

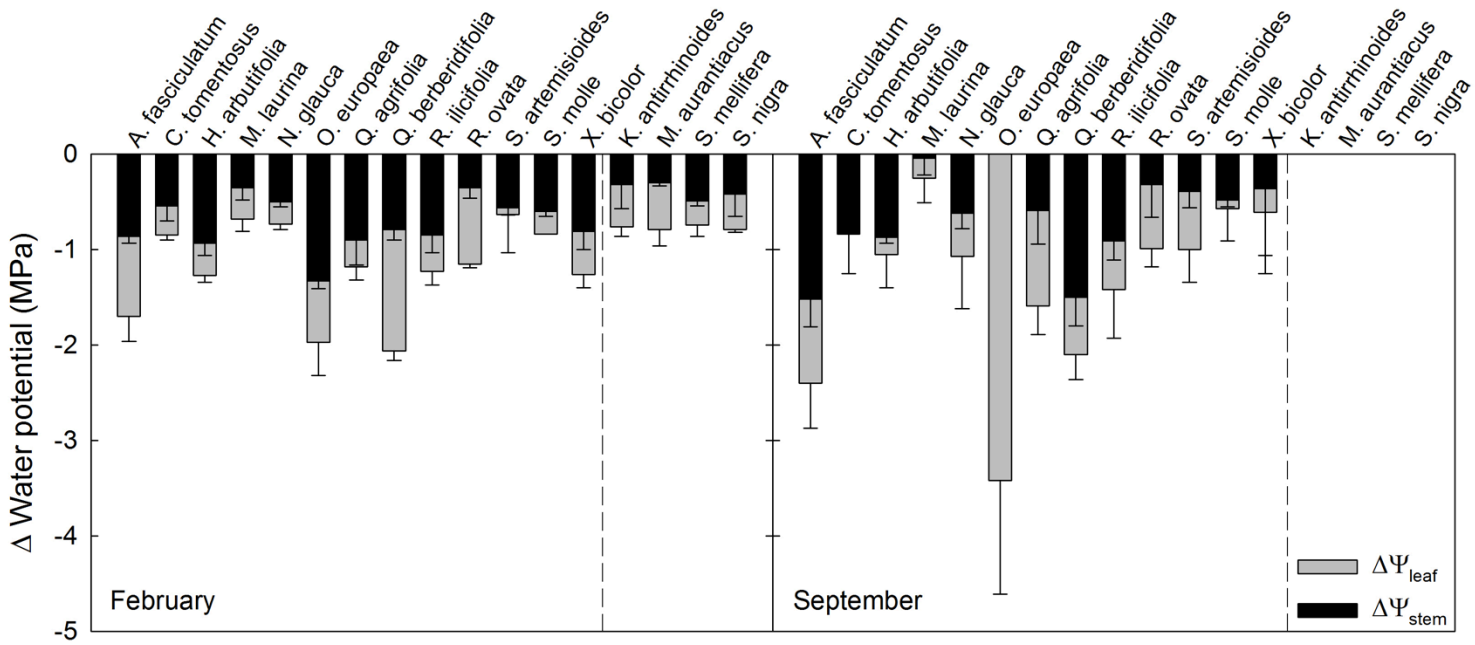

Figure 1.2. Change in water potential from predawn to midday for stems ($\Delta\Psi_{stem}$; black bars) and leaves ($\Delta\Psi_{leaves}$; grey bars) during the wet season (February; left panel) and dry season (September; right panel) in a California Mediterranean-type climate region.

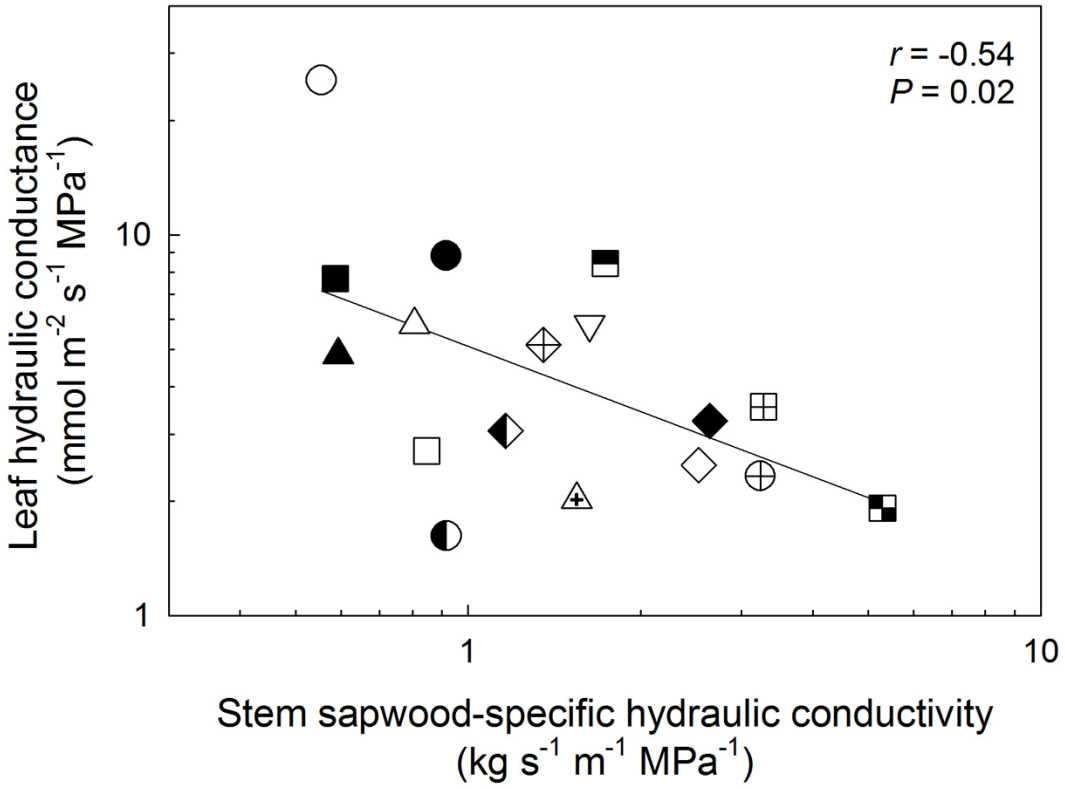

Figure 1.3. Relationship between stem sapwood-specific hydraulic conductivity and leaf hydraulic conductance (n=17) in a California Mediterranean-type climate region. Each symbol represents a different species mean. Corresponding species and symbols are found in Table 1.

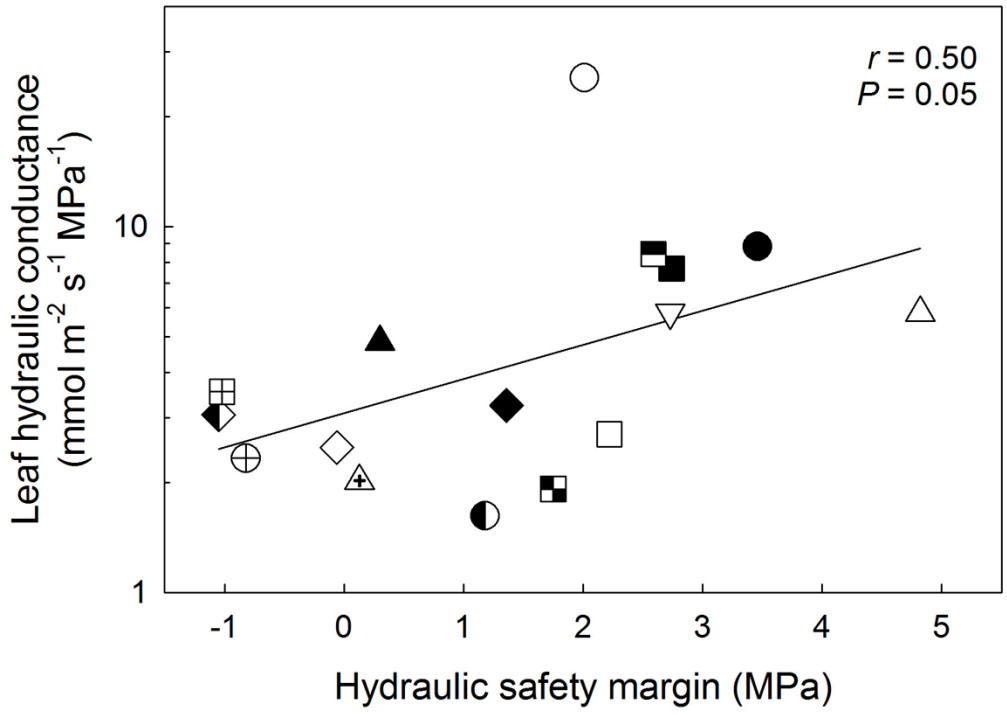

Figure 1.4. Relationship between hydraulic safety margin and leaf hydraulic conductance (*n*=16) in a California Mediterranean-type climate region. Each symbol represents a different species mean. Corresponding species and symbols are found in Table 1.

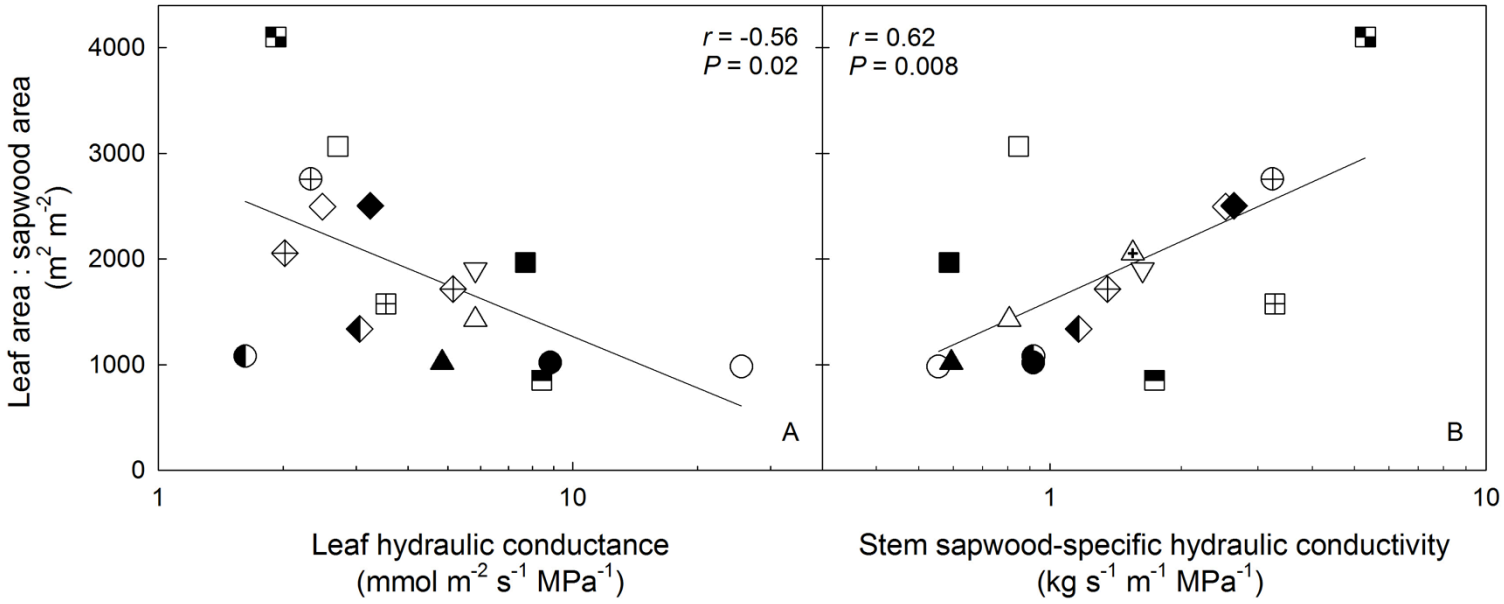

Figure 1.5. Relationship between (a) leaf hydraulic conductance and leaf area to sapwood area ratio (*n*=17), and (b) stem sapwood-specific hydraulic conductivity and leaf area to sapwood area ratio (*n*=17) in a California Mediterranean-type climate region. Each symbol represents a different species mean. Corresponding species and symbols are found in Table 1.

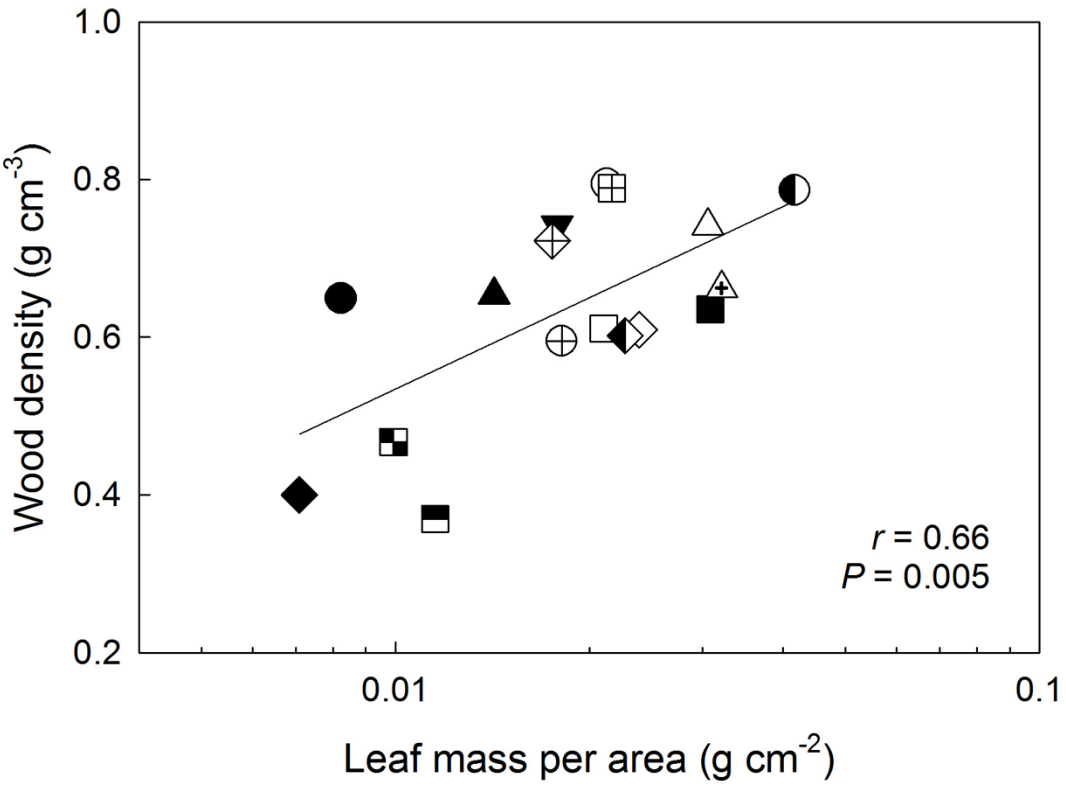

Figure 1.6. Relationship between leaf mass per area and wood density (*n*=17) in a California Mediterranean-type climate region. Each symbol represents a different species means. Corresponding species and symbols are found in Table 1.

Chapter 2: Plant hydraulic responses to long-term dry season nitrogen deposition dictate future drought tolerance in a climate change hotspot

Abstract

Anthropenic nitrogen (N) deposition represents a significant N input for many terrestrial ecosystems. N deposition can affect plants on scales ranging from photosynthesis to community composition, yet few studies have investigated how changes in N availability affect plant water relations. We tested the effects of N addition on leaf hydraulic conductance (K_{leaf}), stem hydraulic conductivity (K_h), xylem vulnerability to cavitation (P_{50}), wood density, photosynthetic gas exchange, and leaf chemistry in a semi-arid ecosystem in southern California using long-term plots fertilized with N for over a decade. The dominant species were *Artemisia californica* and *Salvia mellifera* at Santa Margarita Ecological Reserve and *Adenostoma fasciculatum* and *Ceanothus greggii* at Sky Oaks Field Station. All species showed increased leaf N concentration, yet each species had a differing physiological response to long-term N addition. Dry season $\Psi_{predawn}$ were less negative with N addition for all species except *Adenostoma*, but there were no differences in Ψ_{midday}, nor for wet season water potentials. *Artemisia* was particularly responsive, as N addition increased K_h, stomatal conductance, transpiration, and leaf isotopic composition ($\delta^{13}C$), and decreased SLA and wood density. *Ceanothus* showed increased transpiration with N adition, and all species showed a significant change in foliar $\delta^{15}N$, indicating that added N was taken up by study species. The alteration of water relations and drought resistance parameters with N addition in

Artemisia indicates that N deposition can affect the ability of native southern California shrubs to respond to drought.

Introduction

While the atmosphere is ~78% nitrogen (N), net primary productivity in many terrestrial ecosystems is constrained by N limitation (Vitousek & Howarth, 1991; LeBauer & Treseder, 2008). This is because atmospheric N is relatively inert and must first be fixed before it is biologically useful, which plants alone are incapable of. However, anthropogenic N deposition from industrial fixation, such as in internal combustion engines, has been steadily increasing in recent decades due to rapid urbanization and development, and can deposit anywhere from 25 – 50 kg N ha^{-1} yr^{-1} (Bytnerowicz, 1996; Fenn *et al.*, 2003b). This represents a significant N input for many semi-arid ecosystems (Westman, 1981; Bytnerowicz, 1996; Padgett *et al.*, 1999; Fenn *et al.*, 2003b) and is a primary component of global change (LeBauer & Treseder, 2008) as it can significantly alter ecological communities (Fenn *et al.*, 2003a). For example, while N deposition can increase terrestrial plant productivity (Vitousek & Howarth, 1991), the response is not uniform for all species or even all ecosystems (Matson *et al.*, 2002) because of differences in resource acquisition, resource-use efficiency, allocation, growth responses, and competitive ability (Fenn *et al.*, 2003a; Vourlitis & Pasquini, 2009). Many species are actually adapted to living in low N availability environments (Bobbink *et al.*, 1998), and exhibit defining characteristics including slow growth rates, low photosynthetic rates, and a low capacity for nutrient uptake (Chapin III *et al.*, 1993; EPA, 2005). When N

availability increases, low-N adapted plants cannot compete with nitrophilic plant species that can rapidly take advantage of increased N availability (Fenn *et al.*, 1998). Hence, N deposition leads to loses of diversity (Vitousek *et al.*, 1997; Suding *et al.*, 2005), as is the case with type-conversion from diverse native shrublands to exotic grassland monocultures in southern California (Stylinski & Allen, 1999; Cione *et al.*, 2002; Vilà *et al.*, 2003; Gaertner *et al.*, 2009; Kimball *et al.*, 2014).

While N deposition is one component of environmental change, climate change is another. Average global temperatures have risen in the past several decades due to anthropogenic greenhouse gas emissions, and temperatures are expected to increase by 0.3 to 3.3°C by 2100 (IPCC, 2014). In addition, precipitation patterns are likely to change, leading to longer, more intense, more expansive, and/or more frequent drought events (IPCC, 2014). Global change-type drought is drought that occurs in conjunction with warmer temperatures due to climate change (Breshears *et al.*, 2005), and is already affecting forests on every wooded continent and driving regional mortality (Allen, 2009; Allen *et al.*, 2010b). Regions with seasonally and annually variable climatic conditions, such as the Mediterranean-type ecosystem of California, may be highly susceptible to climate change (Diffenbaugh *et al.*, 2008), and the interaction between anthropogenic climate change and N deposition are unprecedented. Therefore, understanding the interaction between N and water availability in variable environments and how plants respond to this rapid environmental change is important for predicting future changes. For example, (Allen *et al.*, 2010a) examined the effects of chronic N deposition on mature conifers in a piñon-juniper woodland in New Mexico and found that piñon pine

altered its hydraulic architecture by increasing needle biomass and reducing associations with ectomycorrhizal fungi in response to N fertilization, while arbuscular mycorrhizal juniper did not respond similarly. With the onset of drought in 2001, fertilized piñon could not hydraulically support its larger needle biomass and as a result experienced widespread mortality, whereas fertilized juniper and all control plants showed higher survival rates. Hence, the coupling of N enrichment and drought significantly impacted this semi-arid ecosystem. There are also biotic interactions associated with climate change and nutrient addition. For example, plants under intense water stress may not be able to properly allocate resources towards defense, and the ultimate cause of mortality may be attack from pathogens or insects rather than the drought conditions themselves (McDowell *et al.*, 2008; McDowell, 2011). In fact, Eatough Jones et al. (2004) found that ozone exposure and nitrogen deposition led to increased susceptibility to bark beetle attack under drought conditions for pine. Furthermore, phosphorus and potassium addition in tropical tree seedlings increases herbivory, altering the balance of plant-insect interactions (Santiago et al., 2012).

While changes in N availability can alter ecological communities, the mechanisms behind these large-scale shifts may be attributed to plant physiological responses. For example, higher total leaf N is associated with higher rates of CO_2 assimilation (Gulmon & Chu, 1981; Evans, 1989; Pasquini & Santiago, 2012). However, many physiologically-focused studies exam short-term fertilization, seedlings, or only leaf traits. Leaves turn over quickly and thus can capture rapid or more instantaneous responses to changes in nutrient availability. However, other longer-lived organs, such as

woody branches, capture responses to conditions during growth and are maintained until mortality. Hence, woody branches that are composed of many years of growth potentially capture a more integrated response to nutrient changes than leaves, and significant acclimation may not be noticeable except over long-time scales. However, few studies have investigated how changes in N availability affect plant drought adaptation properties, including hydraulic conductivity and vulnerability to cavitation (Harvey & van den Driessche, 1997; Bucci *et al.*, 2006), especially in semi-arid environments prone to drought. This is surprising, given that leaf N concentration, maximum photosynthesis, and other components of the leaf economic spectrum are related to hydraulic conductivity, which is a critical component of overall plant performance (Santiago *et al.*, 2004; Wright *et al.*, 2004; Brodribb, 2009).

This study utilized long-term N fertilization plots (>10 years) to investigate the effects on plant eco-physiological traits related to drought adaptation and hydraulic properties in a seasonally drought prone environment. Within these plots, Vourlitis and Pasquini (2009) found that the relative composition of the coastal sage scrub shrubs *Artemisia californica* increased and *Salvia mellifera* decreased with N addition over time, especially during years with favorable rainfall, but this trend was opposite in dry years (Vourlitis, 2012). There was no significant difference in relative composition of the chaparral shrubs *Adenostoma fasciculatum* or *Ceanothus greggi* between control and fertilization plots. Vourlitis (2012) found that in the chaparral, net primary productivity (NPP) was initially inhibited by N addition, but eventually increased, as it has now been doing consistently. If there are changes in species composition and NPP due to N

addition, what are the physiological mechanisms underlying these changes? We hypothesized that increased relative composition with N addition in *Artemisia* is supported by enhanced gas exchange, increased stem conductivity, and/or changes in functional traits associated with high growth rates such as increased specific leaf area and decreased wood density, whereas decreasing relative composition in *Salvia*, and constant relative composition in *Adenostoma* and *Ceanothus*, is associated with moderate or no change in physiological or functional traits. We also expected that the specific suite of trait adjustments to N addition would indicate whether drought tolerance was enhanced or harmed. If a species does not change its relative composition with long-term N fertilization, then it would likely show few or not trait responses, leading to no significant adjustment in drought tolerance with N addition. However, species that increase rates of physiological processes and growth with increases in resource availability may experience a trade-off and suffer a reduction in drought tolerance with N addition (Grime, 1977; Chapin III, 1991). To test these hypotheses, we measured a suite of 17 physiological traits that describe plant carbon gain, water loss, water status, and drought resistance for these four native California shrub species in control and fertilization plots. Understanding the interacting effects of N deposition and global change-type drought on plant physiological processes is important because these may be the mechanisms behind overall species responses to environmental change.

Methods

Experimental design and study species

Experimental plots were established at Santa Margarita Ecological Reserve (SMER) and Sky Oaks Field Station (SOFS) in 2003 (Table 1). SMER is located on the Riverside – San Diego county line in southern California, USA, and last burned ~40 years ago. SMER is characterized by coastal sage scrub vegetation, the dominant species being *Artemisia californica* Less. and *Salvia mellifera* Greene, which have drought deciduous leaves (Table 2). SOFS is located in northeastern San Diego Country, California, USA, and lasted burned in 2003. SOFS is characterized by chaparral vegetation, the dominant species being *Adenostoma fasciculatum* H. & A. and *Ceanothus greggii* A. Gray, which have evergreen leaves (Table 2).

Each site has eight 10 × 10 m plots, four of which are fertilized with 50 kg N ha^{-1} yr^{-1} in a single application as ammonium nitrate from 2003 – 2006, ammonium sulfate from 2007 – 2009, and urea from 2010 to present each September via a handheld spreader and four of which are un-manipulated control plots, separated by at least a 5 m buffer in a completely randomized design. Background N deposition is estimated at 2 – 3 kg N ha^{-1} yr^{-1} at SOFS and 6 – 8 kg N ha^{-1} yr^{-1} at SMER and from a high-resolution (4 km) model (Tonnesen *et al.*, 2007; Fenn *et al.*, 2010).

Photosynthetic leaf traits

In May and June 2013, photosynthetic gas exchange was measured on 5 – 6 individuals per species per treatment using a LI-6400 portable photosynthesis system (Li-Cor

Biosciences, Lincoln, NE, USA) with a red-blue light source (6400-02B no. SI-710; Li-Cor Biosciences). In the morning (0800 – 1200), leaves were put in the chamber, with photon flux density (PFD; μmol m^{-2} s^{-1}) initially set at 500 (60 sec), then increased to 1000 (60 sec), then 1500 (120 sec). At 1500 μmol m^{-2} s^{-1} PFD, we determined light-saturated rate of photosynthetic CO_2 assimilation per area and mass (A_{area} and A_{mass}), stomatal conductance (g_s), transpiration (E), intrinsic water use efficiency (WUE; A_{area}/g_s), integrated water use efficiency (A_{area}/E), and the ratio of intercellular to ambient CO_2 concentration (C_i/C_a). We then harvested the leaves measured for gas exchange to determine specific leaf area, foliar nitrogen concentration, foliar carbon to nitrogen ratio, and carbon and nitrogen stable isotope ratios. Specific leaf area (SLA), was determined for individual leaves by measuring leaf area using a leaf area meter (LI-3100), drying leaves for 48h at 65°C before measuring dry mass, and dividing dry mass (g) by fresh leaf area (cm^2). Dried leaf samples were then ground in a ball mill (SPEX 8000D Dual Mixer/Mill; Metuchen, NJ). Foliar nitrogen and carbon concentration (%N and %C) and carbon and nitrogen isotopic ratios ($\delta^{13}C$ and $\delta^{15}N$) were determined with an elemental analyzer (ECS 4010; Costech, Valencia, CA, USA) at the Facility for Isotopic Ratio Mass Spectrometry (FIRMS) at the University of California, Riverside, California, USA. Photosynthetic nitrogen use efficiency (PNUE) was calculated by dividing A_{area} by %N.

Plant water potential

Predawn and midday bulk tissue water potentials ($\Psi_{predawn}$ and Ψ_{midday}; MPa) were measured on two individuals per species per plot during the dry season (July 2013) and

wet season (February 2014) with a pressure chamber (Model 1000, Plant Moisture Stress Instruments, Albany, Oregon, USA) to determine plant water status. Upon collection, samples were immediately placed in a plastic bag, sealed, and put in a dark cooler. Sample ends were cleanly cut with a fresh razor blade prior to measurement.

Leaf hydraulic conductance

Leaf hydraulic conductance (K_{leaf}) was measured during May – June 2013 on newly mature leaves from at least six individuals of each species, using the evaporative flux method (Sack et al., 2002; Sack and Scoffoni, 2013). Fresh leaves were severed from branch samples under water with a razor blade and placed in beakers with filtered (0.2 μm), degassed KCl solution so that the petiole was immersed, but the lamina did not come in contact with the solution, and covered with plastic to rehydrate for ~8 hours. Then, leaves were connected to a potometer interfaced with a laptop to record transpiration, with lights arranged above the sample to produce a photon flux density of >1200 μmol m^{-2} s^{-1} to induce stomatal opening, and a fan below the sample to reduce the boundary layer around the leaf. Once steady-state transpiration (*E;* mmol s^{-1}) was achieved, leaves were place in a plastic bag and disconnected from the potometer to measure leaf water potential (Ψ_{leaf}; MPa) with a pressure chamber (Model 1000, Plant Moisture Stress Instruments). Finally, leaf area was measured with a leaf area meter (LI-3100, Li-Cor Biosciences, Lincoln, Nebraska, USA). The leaf hydraulic conductance (K_{leaf}; mmol m^{-2} s^{-1} MPa^{-1}) was calculated as:

$$K_{leaf} = E/\Psi_{leaf} \qquad \text{eqn. (1)},$$

normalized by leaf area.

Stem hydraulic conductance, vulnerability curves, and wood density

Approximately 1m long branch samples were collected from at least six individuals of each species in the field, before being brought back to the lab and cut under water to a length of approximately 18 cm. Emboli were removed from samples by vacuum infiltration under solution for 8 hrs, before recutting and cleanly shaving the sample ends for a final length of 14.2 cm. Stem hydraulic conductivity (K_h) was determined by measuring the gravimetric flow of water through the stem (F; kg s^{-1}) for a given hydraulic head (ΔP; MPa), calculated as:

$$K_h = F \times L / \Delta P \qquad \text{eqn. (2)},$$

where L (m) is the stem length. Stem hydraulic conductivity was also normalized by sapwood area (A_{SW}; m^2) to determine stem sapwood-specific hydraulic conductivity (K_S; kg m^{-1} s^{-1} MPa^{-1}).

Stem xylem vulnerability curves were measured using the centrifuge method (Alder et al., 1997; Jacobsen and Pratt, 2012; Sperry et al., 2012). After determining maximum K_h (K_{max}), stems were spun in a custom built, 14.2 cm diameter rotor in a refrigerated centrifuge (Sorvall RC-5Cplus, Thermo Scientific, Waltham, MA, USA) at increasing speeds to produce negative pressures and induce cavitation. Hydraulic conductivity was measured between each induced pressure, and percent loss of conductivity (PLC) was calculated as:

$$PLC = 100 \times (1 - (K_h / K_{max}) \qquad \text{eqn. (3)}.$$

This was repeated until the stem lost >90% conductivity. Vulnerability curves were constructed by plotting pressure versus PLC and fitting a Weibull model (Pammenter and Willigen, 1998):

$$PLC = 100/(1+\exp(a(\Psi - b))) \quad \text{eqn. (4),}$$

from which the pressure, or water potential, at 50% of conductivity lost (P_{50}) was determined for each species.

Wood density was measured by removing the bark and pith from stem sub-samples and determining the fresh volume with the water displacement method (Williamson & Wiemann, 2010; Osazuwa-Peters *et al.*, 2011), then drying the xylem for 48h at 65°C before measuring dry mass. Woody density (g cm^{-3}) was calculated as the ratio of xylem dry mass (g) to fresh volume (cm^3).

Statisticcal analysis

Student's *t*-test in SAS was used to compare differences in traits between control and N addition treatments for each species. Results were considered significant if $p<0.05$. Differences between sites (time since fire, elevation, soil type, etc.) prohibited site and hence vegetation type (chaparral versus coastal sage scrub) comparisons; hence species responses were compared within each site.

Results

All species showed increased foliar N concentration in the N fertilization plots, indicating increased uptake of N with long-term fertilization (Figure 1). In addition, all species

showed enriched $\delta^{15}N$ (not shown) and decreased C/N (Figure 1) in N fertilization plots except *Ceanothus*, an N-fixer (Table 2) that showed lighter $\delta^{15}N$ and no difference in C/N (Figure 1). *Artemisia* and *Ceanothus* showed increased E in N fertilization plots, and *Artemisia* also showed greater g_s and enriched $\delta^{13}C$ in the N fertilization plots (Figure 2), but there were no corresponding changes in photosynthesis (A_{area} or A_{mass}), WUE, or PNUE for any species, indicating alleviation of N-limitation did not elicit enhanced maximum photosynthetic rate. However, the increased g_s and E of *Artemsia* may be linked to increased stem water transport, as K_h increased and wood density decreased with N addition (Figure 4). Yet, there were no changes in P_{50} or K_{leaf} with N addition, indicating an increased efficiency of water transport without a corresponding decrease in safety. *Artemisia* showed decreased SLA with N addition (Figure 4). All species except *Adenostoma* showed less negative predawn water potentials in N fertilization plots than control plots during the dry season (Figure 3), but there were no differences between treatments for Ψ_{midday} or during the wet season. Overall, *Artemisia* was highly response to alleviation of N-limitation, indicating a nitrophilic functional type. *Adenostoma*, *Ceanothus*, and *Salvia* displayed few trait changes in response to N-fertilization, indicating low-N adapted functional types.

Discussion

Our data indicate that rather than a convergent response to N addition for all four Mediterranean-type shrubs, there were differing physiological responses to alleviation of N limitation, revealing contrasting functional groups. All four species exhibited increased

foliar N with N addition and all species except *Ceanothus* exhibited decreased C/N ratios with N addition, consistent with uptake of additional N with fertilization. However, while all species acquired more N in N-fertilization plots, the physiological responses among species were not similarly uniform. For example, *Artemisia* was a particularly responsive species, as E, g_s, $\delta^{13}C$, SLA, K_h, and wood density all changed with the addition of N, indicating a nitrophilic functional type. However, *Adenostoma*, *Ceanothus*, and *Salvia* displayed few physiological adjustments with N addition, indicating they have a low-N adapted functional type. The lack of significant physiological changes with N fertilization for *Adenostoma*, *Ceanothus*, and *Salvia* point to no alterations in drought adaptation for these species. *Artemisia*, however, displayed traits of increased water use, including increased E, g_s, K_h, and decreased wood density, which may confer a competitive advantage during favorable times, but may be detrimental under drought conditions, especially in this region with seasonally and annually variable climatic conditions that may be exacerbated in a climate change hotspot (Diffenbaugh *et al.*, 2008).

We expected that increased N would greatly enhance gas exchange, including increased photosynthesis and water use efficiency, if species were nitrophilic. However, we found no difference in A_{area}, A_{mass}, intrinsic or integrated WUE, or PNUE between control and N fertilization plots for any species. The only response related to photosynthesis was an increase in leaf $\delta^{13}C$ in *Artemisia*, indicating that increased leaf N on average reduced intercellular CO_2 concentration through CO_2 uptake by Rubisco. Yet the lab of responses of other photosynthetic parameters to N addition are in contrast to the much more common finding that maximum photosynthetic rate is limited by N in a

variety of ecosystems (Clearwater & Meinzer, 2001). Yet, our study differs from many others in that it represents a semi-arid ecosystem that receives most precipitation during the winter months, resulting in an annual seasonal water deficit. In addition, high interannual variability leads to extended rainless periods. Therefore when water is in short supply, it may limit the ability of species to exploit increasing N availability for increasing maximum rates of photosynthesis and reveal alternate strategies for regulating gas exchange and balancing water, nutrient, and carbon economics. Findings similar to this were reported in a water and nutrient addition study for *Arbutus unedo*, an evergreen Mediterranean shrub; the only effect of nutrient addition was an increase in leaf nutrient content (Castell & Terradas, 1994). In addition, Cregger et al. (2014) found soil N concentration increased when water availability decreased, also suggesting plants and microbes are inactive during dry times and are therefore unable to use the nutrient resource. Our results that *Artemisia* increased g_s, and increased E, and *Ceanothus* showed increased E with N addition (Figure 2), further indicate that the relative responses of photosynthesis and stomatal conductance, and their subsequent effects on long-term integrated intercellular CO_2 differed. *Artemisia* also demonstrated coordinated changes between gas exchange and hydraulic traits, as demonstrated by increased, g_s, E, and K_h.

We expected that long-term increased N availability would alter plant hydraulic properties for nitrophilic species, capturing an integrated response especially in wood-related traits. All species except *Adenostoma* showed less negative $\Psi_{predawn}$ during the dry season in N fertilization plots, possibly indicating increased access to water (Bhaskar & Ackerly, 2006) with fertilization (Figure 3B). This trend is opposite of what is expected

based on studies showing that fertilization can reduce plant allocation to belowground biomass and hence decrease root access to water (Aerts *et al.*, 1991; Allen *et al.*, 2010a). On the other hand, when nutrients are limiting, roots can proliferate in nutrient-rich patches (Hodge, 2004). The differences in $\Psi_{predawn}$ between N addition and control plots disappeared by midday, potentially because of greater water use in fertilization plots. However, only *Artemisia* and *Ceanothus* had increased E or g_s in fertilization plots that could potentially compensate for predawn differences, and no species showed differences in instantaneous WUE (A/g_s). *Artemisia* also showed increased K_h and decreased wood density in response to N addition, which may be related to its greater water use and/or increased growth rate (Vourlitis, 2012), as similarly found for mangroves fertilized with N (Lovelock *et al.*, 2004). There were no differences in these traits for the other three study species, or for P_{50} or K_{leaf} for any species, which is in contrast to previous studies on Cerrado savannah trees that showed five years of N fertilization increased sapwood-specific stem conductivity, decreased wood density, and increased xylem resistance to cavitation (Bucci *et al.*, 2006). The lack of a change in K_{leaf} with increased N availability in our study is interesting given that leaves are highly dynamic. However, another study that added N and phosphorus for five species in a semi-deciduous Atlantic forest in Argentina found that K_{leaf} responses to nutrient addition were species-specific (Villagra *et al.*, 2013). For *Artemisia*, the increase in K_h, but lack of change in P_{50}, displays an adjustment in efficiency of water movement without a corresponding change in safety, which would be disadvantageous under severe drought conditions. This was seen by (Vourlitis, 2012), who found a significant interaction between rainfall and N in our

coastal sage scrub experimental plots, with *Artemisia* increasing in percent cover and *Salvia* decreasing in percent cover during favorable precipitation years, and the opposite trend during drought periods.

We expected to find increased physiological functioning with higher N availability if species were nitrophilic. However, the nature of the experimental design does not control for competition between co-occurring species within a plot or within treatments. Therefore, while we might have expected *Artemisia* and *Salvia*, both coastal sage scrub shrubs, to respond positively to N addition, physiological differences between these two species means a higher positive response in one species (*Artemisia*) may have a negative effect on the co-occurring species (*Salvia*), that cannot respond at the same (Vourlitis & Pasquini, 2009). For example, in a study done by Gray and Schlesinger (1983), the drought deciduous coastal sage scrub species *Salvia leucophylla* responded positively to N fertilization when grown in isolation in pots, displaying a greater relative growth rate and greater leaf area compared to the control treatment. However, if *Salvia* were grown in competition, as is the case with our experimental design, the same "responsive, opportunistic pattern" of physiological changes with nutrient addition may not have been seen. Therefore, it seems that *Artemisia* can respond more quickly and/or at higher rates than *Salvia*, which may be why we did not see that same enhanced physiological functioning for *Salvia* in our experiment. In the chaparral, we saw no change for *Ceanothus* or *Adenostoma* with regard to hydraulic traits. While previous studies found enhanced growth with fertilization in chaparral, especially for *Adenostoma fasciculatum*, we did not find physiological changes with nutrient addition. However,

Gray and Schlesinger (1983) found results similar to our study, with *Ceanothus megacarpus* having an "asymptotic response to increasing nitrogen concentration" and growth that was uncoupled from nitrogen availability. The response of *Ceanothus* to increased N may be linked to its N-fixing ability. In addition, our chaparral site is still recovering from the 2003 Coyote fire, so the dynamics at this site may continue to change as the system recovers.

As mentioned previously, all study species showed increased %N with N addition, and all species except *Ceanothus* showed decreased C/N and enriched $\delta^{15}N$ with fertilization. *Ceanothus* displayed depleted $\delta^{15}N$ with fertilization. While we expected the vegetative $\delta^{15}N$ signature to match that of the fertilizer, the differences we found may in fact be due to the mycorrhizal associations of each species (Table 2). *Adenostoma*, which can switch between arbuscular mycorrhizae (AM) and ectomycorrhiza (EM; Allen *et al.*, 1999) appears to be shifting from EM fractionation to instead to acquire applied nitrogen, as AM *Salvia* is doing. AM *Artemisia's* high physiological activity may promote its need to acquire older, enriched N in the soil. *Ceanothus* is a N-fixer, and appears to be taking up the lighter isotopes of N. Overall, however, we need a better understanding of N cycling in this semi-arid ecosystem.

Artemisia follows a 'live fast, die young' strategy and has a nitrophilic functional type in response to N addition. When N is highly available and rainfall conditions are favorable, *Artemisia's* growth rate increases (Vourlitis 2012) as explained by its physiological adjustments. This untempered growth makes it highly competitive as it outcompetes *Salvia* for relative composition in the N addition plots. However, the

physiological alterations that led to *Artemisia's* untempered growth and competitive nature also lead to its downfall during unfavorable conditions. With N addition, *Artemisia* 'outgrows' its ability to withstand drought conditions and experiences high mortality during these rainless periods, allowing for the co-occurring *Salvia* to catch up, similar to the case of piñon-pine and juniper in Allen et al. (2010b). This may be why there is type conversion in coastal sage scrub: *Artemisia* growth rate increases, but it cannot hydraulically support itself during periods of drought and hence experiences high mortality, which allows exotic grasses to invade (Padgett *et al.*, 1999). The lack of physiological or functional trait responses to N addition for *Adenostoma*, *Ceanothus*, and *Salvia* also means that their drought tolerance is not reduced, which will be important under the predicted future climate conditions for this region. Water limitation may also play a part in the dynamics we observed for *Adenostoma*, *Ceanothus*, and *Salvia*. Kimball et al. (2014) conducted a precipitation and nutrient manipulation experiment in California coastal sage scrub, and found that with only increased water, native shrub cover increased; decreased water availability and increased N resulted in decreased native shrub cover and type conversion. Overall, however, chaparral and coastal sage scrub communities are in semi-arid environments and they are operating under more extreme conditions than mesic vegetation communities. Therefore, they may be less able to move along the trade-off continuum between fast growth and less stress tolerance at one end of the spectrum, and slow but growth higher stress tolerance due to the lack of physiological adjustments in response to N availability at the other end.

References

Aerts R, Boot RGA, van der Aart PJM. **1991**. The relation between above- and belowground biomass allocation patterns and competitive ability. *Oecologia* **87**: 551–559.

Allen CD. **2009**. Climate-induced forest dieback: an escalating global phenomenon. *Unasylva* **231**: 60.

Allen MF, Allen EB, Lansing JL, Pregitzer KS, Hendrick RL, Ruess RW, Collins SL. **2010a**. Responses to chronic N fertilization of ectomycorrhizal piNon but not arbuscular mycorrhizal juniper in a piNon-juniper woodland. *Journal of Arid Environments* **74**: 1170–1176.

Allen MF, Egerton-Warburton LM, Allen EB, Karen O. **1999**. Mycorrhizae in Adenostoma fasciculatum Hook. and Arn.: A combination of unusual ecto- and endo-forms. *Mycorrhiza* **8**: 225–228.

Allen CD, Macalady AK, Chenchouni H, Bachelet D, McDowell NG, Vennetier M, Kitzberger T, Rigling A, Breshears DD, Hogg EHT, *et al.* 2010b. A global overview of drought and heat-induced tree mortality reveals emerging climate change risks for forests. *Forest Ecology and Management* **259**: 660–684.

Bhaskar R, Ackerly DD. **2006**. Ecological relevance of minimum seasonal water potentials. *Physiologia Plantarum* **127**: 353–359.

Bobbink R, Hornung M, Roelofs JGM. **1998**. The effects of air-borne nitrogen pollutants on species diversity in natural and semi-natural European vegetation. *Journal of Ecology* **86**: 717–738.

Breshears DD, Cobb NS, Rich PM, Price KP, Allen CD, Balice RG, Romme WH, Kastens JH, Floyd ML, Belnap J, *et al.* 2005. Regional vegetation die-off in response to global-change-type drought. *Proceedings of the National Academy of Sciences of the United States of America* **102**: 15144–15148.

Brodribb TJ. **2009**. Xylem hydraulic physiology: The functional backbone of terrestrial plant productivity. *Plant Science* **177**: 245–251.

Bucci SJ, Scholz FG, Goldstein G, Meinzer FC, Franco AC, Campanello PI, Villalobos-vega R, Bustamante M, Miralles-Wilhelm F. **2006**. Nutrient availability constrains the hydraulic architecture and water relations of savannah trees. *Plant, Cell & Environment* **29**: 2153–2167.

Bytnerowicz A. **1996**. Nitrogen deposition in California forests: A review. *Environmental Pollution* **92**: 127–146.

Castell C, Terradas J. **1994**. Effects of water and nutrient availability on water relations, gas exchange and growth rate of mature plants and resprouts of Arbutus unedo L. *Annals of Botany* **73**: 595–602.

Chapin III FS. **1991**. Integrated Responses of Plants to Stress. *BioScience* **41**: 29–36.

Chapin III FS, Autumn K, Pugnaire F. **1993**. Evolution of suites of traits in response to environmental stress. *American Naturalist*: 78–92.

Cione NK, Padgett PE, Allen EB. **2002**. Restoration of native shrubland impacted by axotic grases,frequent fire, and nitrogen deposition in southern califonia. *Restoration Ecology* **10**: 376–384.

Clearwater MJ, Meinzer FC. **2001**. Relationships between hydraulic architecture and leaf photosynthetic capacity in nitrogen-fertilized Eucalyptus grandis trees. *Tree Physiology* **21**: 683–690.

Cregger MA, McDowell NG, Pangle RE, Pockman WT, Classen AT. **2014**. The impact of precipitation change on nitrogen cycling in a semi-arid ecosystem (S Niu, Ed.). *Functional Ecology* **28**: 1534–1544.

Diffenbaugh NS, Giorgi F, Pal JS. **2008**. Climate change hotspots in the United States. **35**: L16709.

Eatough Jones M, Paine TD, Fenn ME, Poth M a. 2004. Influence of ozone and nitrogen deposition on bark beetle activity under drought conditions. *Forest Ecology and Management* **200**: 67–76.

Egerton-Warburton LM, Querejeta JI, Allen MF. **2007**. Common mycorrhizal networks provide a potential pathway for the transfer of hydraulically lifted water between plants. *Journal of Experimental Botany* **58**: 1473–1483.

EPA. **2005**. *Review of the national ambient air quality standards for particulate matter: Policy assessment of scientific and technical information*.

Evans JR. **1989**. Photosynthesis and nitrogen relationships in leaves of C3 plants. *Oecologia* **78**: 9–19.

Fenn ME, Allen EB, Weiss SB, Jovan S, Geiser LH, Tonnesen GS, Johnson RF, Rao LE, Gimeno BS, Yuan F, *et al.* 2010. Nitrogen critical loads and management

alternatives for N-impacted ecosystems in California. *Journal of environmental management* **91**: 2404–2423.

Fenn M, Baron JS, Allen EB, Rueth HM, Nydick KR, Geiser L, Bowman WD, Sickman JO, Meixner T, Johnson DW, *et al.* 2003a. Ecological effects of nitrogen deposition in the western United States. *BioScience* **53**: 404–420.

Fenn M, Haeuber R, Tonnesen GS, Baron JS, Grossman-Clarke S, Hope D, Jaffe DA, Copeland S, Geiser L, Rueth HM, *et al.* 2003b. Nitrogen Emissions, Deposition, and Monitoring in the Western United States. *BioScience* **53**: 391.

Fenn ME, Poth M a, Aber JD, Baron JS, Bormann BT, Johnson DW, Lemly a D, Mcnulty SG, Ryan DF, Stottlemyer R. **1998**. Nitrogen Excess in North American Ecosystems : Predisposing Factors , Ecosystem Responses , and Management Strategies. *Ecological Applications* **8**: 706–733.

Gaertner M, Den Breeyen a., Cang Hui, Richardson DM. **2009**. Impacts of alien plant invasions on species richness in Mediterranean-type ecosystems: a meta-analysis. *Progress in Physical Geography* **33**: 319–338.

Gray JT, Schlesinger WH. **1983**. Nutrient use by Evergreen and Deciduous Shrubs in Southern California: II. Experimental Investigations of the Relationship between Growth, Nitrogen Uptake and Nitrogen Availability. *The Journal of Ecology*: 43–56.

Gulmon SL, Chu CC. **1981**. The effects of light and nitrogen on photosynthesis, leaf characteristics, and dry matter allocation in the chaparral shrub, Diplacus aurantiacus. *Oecologia* **49**: 207–212.

Harney SK, Edwards FS, Allen MF. **2014**. californica of arbuscular mycorrhizal Identification fungi from Artemisia using the polymerase chain reaction. **89**: 547–550.

Harvey HP, van den Driessche R. **1997**. Nutrition, xylem cavitation and drought resistance in hybrid poplar. *Tree Physiology* **17**: 647–654.

Hodge A. **2004**. The plastic plant: Root responses to heterogeneous supplies of nutrients. *New Phytologist* **162**: 9–24.

IPCC. **2014**. *Climate Change 2014: Impacts, Adaptation, and Vulnerability. Part A: Global and Sectoral Aspects. Contributions of Working Group II to the Fifth Assessment Report of the Intergovernmental Panal on Climate Change.* (CB Field, V Barros, DJ Dokken, KJ Mach, MD Mastrandrea, TE Bilir, M Chatterjee, KL Ebi, YO Estrada, RC Genova, *et al.*, Eds.). Cambridge, UK: Cambridge University Press.

Kimball S, Goulden ML, Suding KN, Parker S. **2014**. Altered Water and Nitrogen Input Shifts Succession in a Southern California Coastal Sage Community. *Ecological Applications*: 140121103535007.

Knecht AA. **1971**. *Soil Survey for Western Riverside Area California.* Washington, DC.

LeBauer DS, Treseder KK. **2008**. Nitrogen limitation of net primary productivity in terrestrial ecosystems is globally distributed. *Ecology* **89**: 371–379.

Lovelock CE, Feller IC, McKee KL. **2004**. The effect of nutrient enrichment on growth, photosynthesis and hydraulic conductance of dwarf mangroves in Panama. *Functional* ….

Matson PA, Lohse KA, Hall SJ. **2002**. The globalization of nitrogen deposition: consequences for terrestrial ecosystems. *Ambio* **31**: 113–119.

McDowell NG. **2011**. Mechanisms Linking Drought, Hydraulics, Carbon Metabolism, and Vegetation Mortality. *Plant Physiology* **155**: 1051–1059.

McDowell NG, Pockman WT, Allen CD, Breshears DD, Cobb NS, Kolb T, Plaut JA, Sperry JS, West AG, Williams DG, *et al.* 2008. Mechanisms of plant survival and mortality during drought: why do some plants survive while others succumb to drought? *New Phytol.* **178**: 719–739.

Moreno JM, Oechel WC. **1992**. Factors controlling postfire seedling establishment in southern California chaparral. *Oecologia* **90**: 50–60.

Osazuwa-Peters O, Zanne AE, contributors P. **2011**. Wood density. *PrometheusWiki*.

Padgett PE, Allen EB, Bytnerowicz A. **1999**. Changes in soil inorganic nitrogen as related to atmospheric nitrogenous pollutants in southern California. *Atmospheric Environment*.

Pasquini SC, Santiago LS. **2011**. Nutrients limit photosynthesis in seedlings of a lowland tropical forest tree species. *Oecologia* **168**: 311–319.

Santiago LS, Goldstein G, Meinzer FC, Fisher JB, Machado K, Woodruff DR, Jones TJ. **2004**. Leaf photosynthetic traits scale with hydraulic conductivity and wood density in Panamanian forest canopy trees. *Oecologia* **140**: 543–550.

Santiago LS, Wright SJ, Harms KE, Yavitt JB, Korine C, Garcia MN, Turner BL. **2011**. Tropical tree seedling growth responses to nitrogen, phosphorus and potassium addition. *Journal of Ecology*: no–no.

Stylinski CD, Allen EB. **1999**. Lack of native species recovery following severe exotic disturbance in southern Californian shrublands. *Journal of Applied Ecology* **36**: 544–554.

Suding KN, Collins SL, Gough L, Clark C, Cleland EE, Gross KL, Milchunas DG, Pennings S. **2005**. Functional- and abundance-based mechanisms explain diversity loss due to N fertilization. *Proceedings of the National Academy of Sciences* **102**: 4387–4392.

Tonnesen GS, Wang Z, Omary M, Chien CJ. **2007**. *Assessment of nitrogen depostion: modeling and habitat assessment.* California Energy Commission, PIER Energy-Related Environmental Research.

Vilà M, Burriel JA, Pino J, Chamizo J, Llach E, Porterias M, Vives M. **2003**. Association between Opuntia species invasion and changes in land-cover in the Mediterranean region. *Global Change Biology* **9**: 1234–1239.

Villagra M, Campanello PI, Bucci SJ, Goldstein G. **2013**. Functional relationships between leaf hydraulics and leaf economic traits in response to nutrient addition in subtropical tree species. *Tree Physiology* **33**: 1308–1318.

Vitousek PM, Aber JD, Howarth RW, Likens GE, Matson PA, Schindler DW, Schlesinger WH, Tilman DG. **1997**. Human alteration of the global nitrogen cycle: sources and consequences. *Ecological Applications* **7**.

Vitousek PM, Howarth RW. **1991**. Nitrogen limitation on land and in the sea: how can it occur? *Biogeochemistry* **13**: 87–115.

Vourlitis GL. **2012**. Aboveground net primary production response of semi-arid shrublands to chronic experimental dry-season N input. *Ecosphere* **3**: art22.

Vourlitis GL, Pasquini SC. **2009**. Experimental dry-season N deposition alters species composition in southern Californian mediterranean-type shrublands. *Ecology* **90**: 2183–2189.

Vourlitis GL, Pasquini S, Zorba G. **2007a**. Plant and soil N response of southern Californian semi-arid shrublands after 1 year of experimental N deposition. *Ecosystems* **10**: 263–279.

Vourlitis GL, Zorba G. **2006**. Nitrogen and carbon mineralization of semi-arid shrubland soil exposed to long-term atmospheric nitrogen deposition. *Biology and Fertility of Soils* **43**: 611–615.

Vourlitis GL, Zorba G, Pasquini SC, Mustard R. **2007b**. Chronic Nitrogen Deposition Enhances Nitrogen Mineralization Potential of Semiarid Shrubland Soils. *Soil Science Society of America Journal* **71**: 836–842.

Westman WE. **1981**. Diversity Relations and Succession in Californian Coastal Sage Scrub. *Ecology* **62**: 170.

Williamson GB, Wiemann MC. **2010**. Measuring wood specific gravity…Correctly. *American Journal of Botany* **97**: 519–524.

Wright IJ, Reich PB, Westoby M, Ackerly DD, Baruch Z, Bongers F, Cavender-Bares J, Chapin T, Cornelissen JHC, Diemer M, *et al.* 2004. The worldwide leaf economics spectrum. *Nature* **428**: 821–827.

Table 2.1. Location and selected characteristics for the Santa Margarita Ecological Reserve (SMER) and Sky Oaks Field Station (SOFS) study sites. Temperature and rainfall data obtained from the Western Regional Climate Center for Ranchita and Oak Grove (SOFS) and the Santa Rosa Plataeu (SMER) from 2003 – 2013 (Vourlitis *et al.*, 2007b) . Soil parent material and taxonomy for SOFS from (Moreno & Oechel, 1992) and for SMER from (Knecht, 1971). Soil bulk density from (Vourlitis *et al.*, 2007a). Soil data from (Vourlitis & Zorba, 2006), sampled in September 2002 for the upper 0 – 10 cm soil layer (mean ± SE, n = 4).

Characteristic	**SMER**	**SOFS**
Latitude and longitude	33°29', 117°09'	33°21', 116°34'
Vegetation	Coastal sage scrub	Chaparral
Elevation, m	338	1418
Mean temperature, °C	16.3	15.8
Annual rainfall, cm	33	57
Soil texture class	Sandy clay loam	Sandy loam
Soil taxonomy	Lithic Haploxeroll	Ultic Haploxeroll
Soil parent material	Igneous and weather Gabbro	Micaceous schist
Bulk density, g cm^{-3}	1.22	1.34
Soil N, mg N g^{-1}	0.86±0.10	0.71±0.05
Soil C, mg C g^{-1}	12.3±1.5	17.0±1.1

Table 2.2. Selected characteristics of four Mediterranean-type shrub species from the Santa Margarita Ecological Reserve (SMER) and Sky Oaks Field Station (SOFS). Abbreviations: Arbuscular mycorrhizae (AM); Ectomycorrhizal (EM). Mycorrhizal association data for *Adenostoma* from (Allen *et al.*, 1999), for *Artemisia* from (Harney *et al.*, 2014), and for *Salvia* from (Egerton-Warburton *et al.*, 2007).

Species	Field site	Vegetation type	Leaf phenology	Leaf type	Mycorrhizal association
Adenostoma fasciculatum	SOFS	Chaparral	Evergreen	Needle-like	AM, EM
Artemisia californica	SMER	Coastal sage scrub	Drought deciduous	Needle-like	AM
Ceanothus greggi	SOFS	Chaparral	Evergreen	Broad	N fixer
Salvia mellifera	SMER	Coastal sage scrub	Drought deciduous	Broad	AM

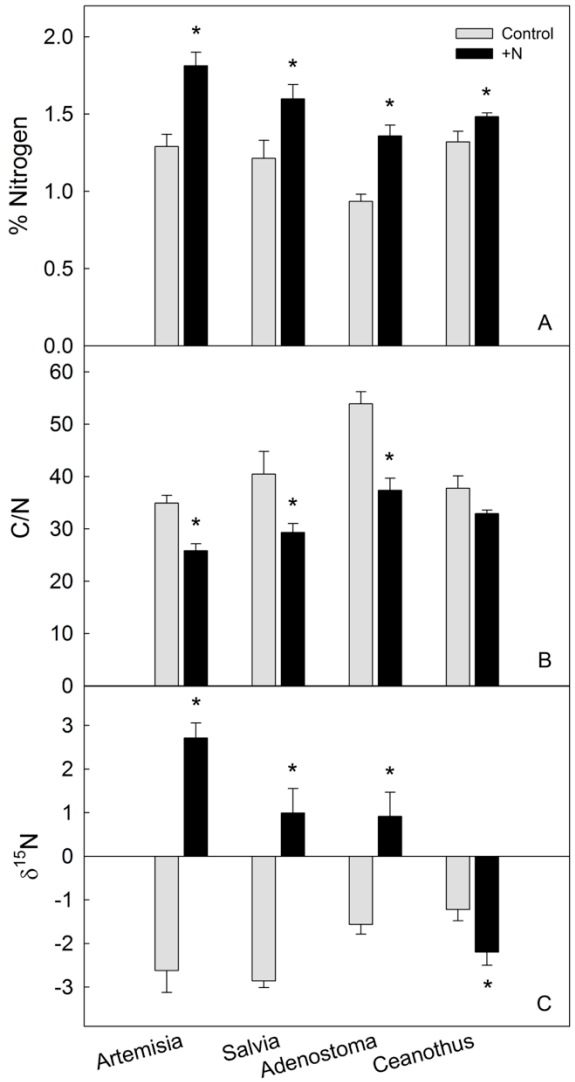

Figure 2.1. Changes in percent foliar nitrogen (% nitrogen; A), carbon to nitrogen ratio (C/N; B), and $\delta^{15}N$ (C) for four Mediterranean shrubs in response to long-term nitrogen fertilization. Control results are reported in grey bars and nitrogen fertilization results are reported in black bars. Mean values are reported ± SE. * indicates statistical significance of $p < 0.05$.

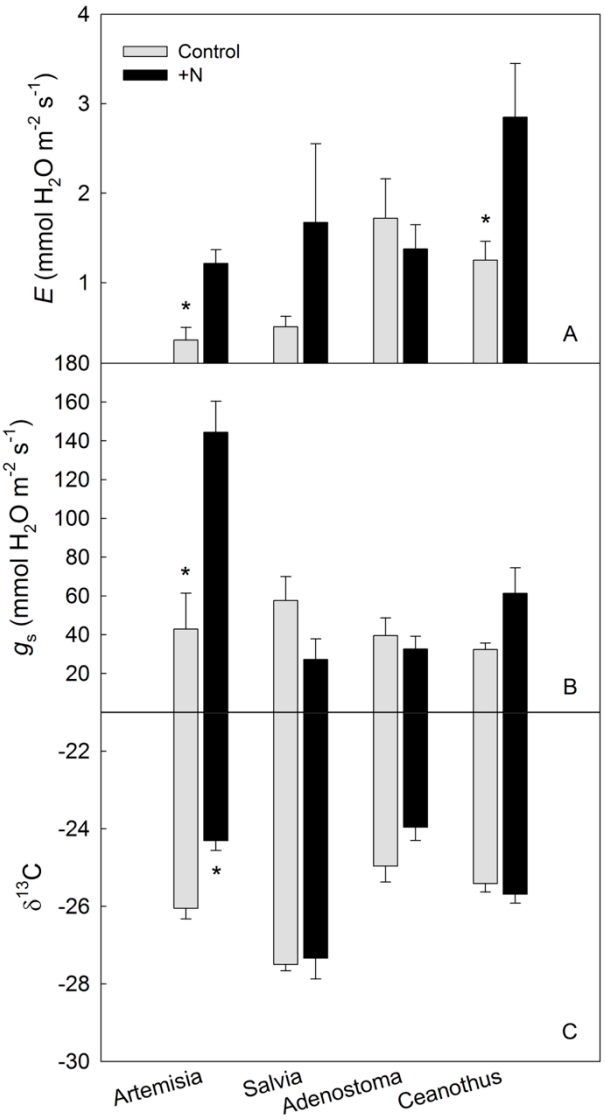

Figure 2.2. Changes in transpiration (*E*; A), stomatal conductance (g_s; B), and $\delta^{13}C$ (C) for four Mediterranean shrubs in response to long-term nitrogen fertilization. Control results are reported in grey bars and nitrogen fertilization results are reported in black bars. Mean values are reported ± SE. * indicates statistical significance of $p < 0.05$.

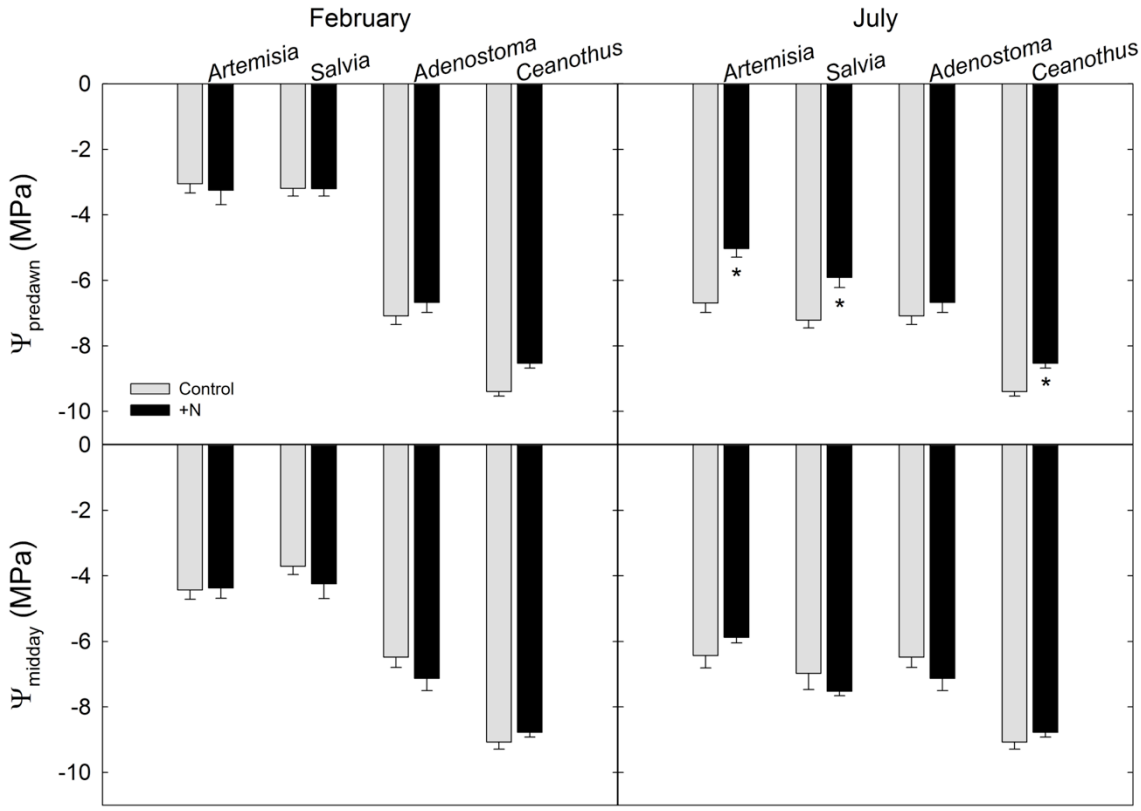

Figure 2.3. Changes in predawn and midday water potentials ($\Psi_{predawn}$ and Ψ_{midday}) during the wet season (February) and dry season (July) for four Mediterranean shrubs in response to long-term nitrogen fertilization. Control results are reported in grey bars and nitrogen fertilization results are reported in black bars. Mean values are reported ± SE. * indicates statistical significance of $p < 0.05$.

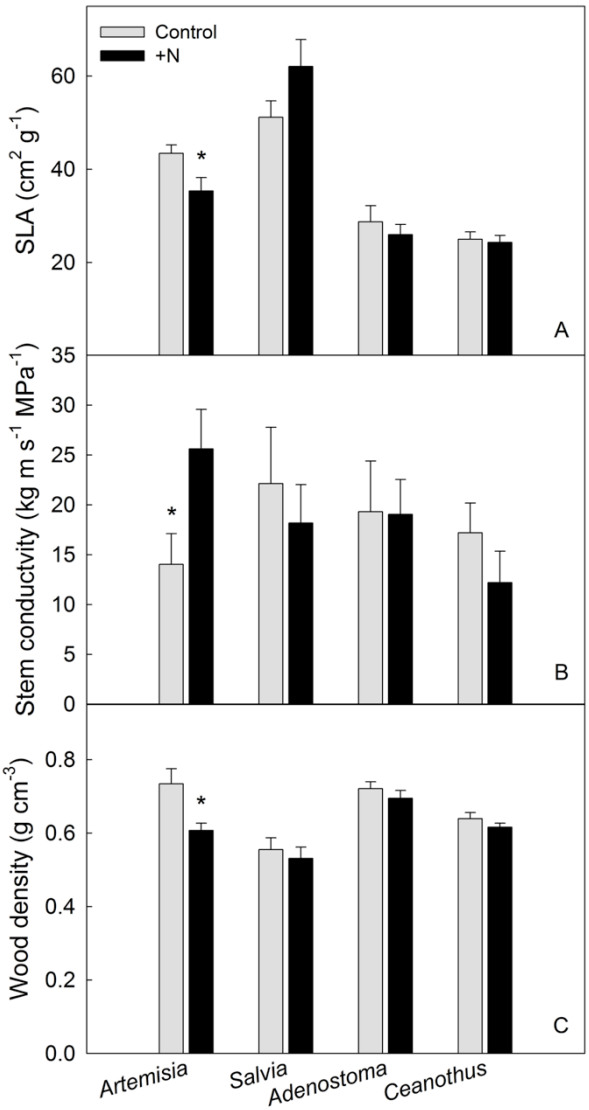

Figure 2.4. Changes in specific leaf area (SLA; A), stem conductivity (B), and wood density (C) for four Mediterranean shrubs in response to long-term nitrogen fertilization. Control results are reported in grey bars and nitrogen fertilization results are reported in black bars. Mean values are reported ± SE. * indicates statistical significance of $p < 0.05$.

Chapter 3: Testing the 'Champagne effect' using the Cavitron technique to measure xylem water extraction curves

Abstract

Plant resistance to drought-induced cavitation is a major drought adaptation trait and is essential to characterizing vulnerability to climate change. This trait is determined using xylem vulnerability curves to calculate the water potential at which 50% of hydraulic conductivity is lost. In the past decade, new techniques have increased the ease and speed at which vulnerability curves are produced. However, these new techniques are also subject to new artifacts, especially as related to long-vesselled species. We investigated one potential mechanism behind the open vessel artifact in centrifuged-based vulnerability curves: the Champagne effect. The Champagne effect hypothesizes that microbubbles introduced to open vessels, either through sample flushing or injection of solution, travel by buoyancy towards the axis of rotation where they artifactually nucleate cavitation. To test the Champagne effect, we constructed vulnerability curves using three different rotor sizes for five species with varying maximum vessel length, as well as water extraction curves that are constructed without injection of solution into the rotor. We found that indeed the Champagne effect may be a major factor in the open vessel artifact.

Introduction

The ability of plants to resist cavitation and endure periods of water deficit is critical for survival under future climate conditions (Brodribb & Cochard, 2009; Brodribb *et al.*, 2010; Choat *et al.*, 2012; Urli *et al.*, 2013). Climate change models predict that extreme climatic events, such as exceptional drought, may become more frequent, more expansive, more intense, or last longer in the future (IPCC, 2014). These extreme events may push species past critical thresholds, leading to reduced physiological functioning and/or mortality. Regional forest mortality events in response to global climate change-type drought have already been reported on every wooded continent (Allen *et al.*, 2010). Negative consequences of regional forest mortality include altered carbon and water cycling and biodiversity losses. Hence understanding how plants cope with drought is important for understanding which species or regions may be most vulnerable.

Vulnerability to xylem cavitation is a linchpin trait in characterizing overall plant drought adaptation strategies (Alder *et al.*, 1997). Maintaining adequate water transport within the plant from roots to shoots to leaves is essential for nearly all major functions (Santiago *et al.*, 2004; Brodribb, 2009). Catastrophic disruptions within this system can have negative physiological consequences leading to hydraulic failure and mortality (Sperry & Tyree, 1988; Brodribb & Cochard, 2009; Brodribb *et al.*, 2010; Urli *et al.*, 2013). During periods of drought, water potentials within the xylem can drop to critical thresholds leading to cavitation, or air-filled spaces that disrupt water transport within the xylem conduits. Different species have different critical water potential thresholds

beyond which cavitation occurs. Typically, the water potential at which 50% of hydraulic conductivity is lost (P_{50}) is used to compare this resistance between species.

P_{50} is calculated from a vulnerability curve (Figure 1), which plots the change in percent loss of conductivity as a function of xylem water potential. There are three principles techniques for inducing cavitation in samples, including bench dehydration, air injection, and centrifugation (Cochard *et al.*, 2013). Centrifugation-generated vulnerability curves can be constructed using a static rotor or a flow rotor known as the Cavitron. With the static rotor, samples are spun at known speeds to induce a pressure or water potential and then removed from the rotor to measure hydraulic conductivity gravimentrically. In the Cavitron, samples are also spun at known speeds to induce a pressure or water potential, but instead of removing the sample from the rotor to measure conductivity in-between pressure steps, water is injected into the Cavitron to measure flow through the sample while it is spinning. Centrifuge-generated vulnerability curves can be constructed much more quickly and with less plant material than the original "gold standard" bench dehydration method. Additionally, by eliminating the need to remove and re-mount samples in between each pressure step, the Cavitron has the major advantages of speed and the ease at which vulnerability curves can be generated, allowing high throughput. Direct comparison of the bench dehydration, static rotor, and Cavitron show they produce similar results across a wide range of xylem functional types; the only exception is for long-vesselled species (Cochard *et al.*, 2005; Li *et al.*, 2008).

Recent tests of the centrifuge technique against other independent techniques, including non-invasive methods, have shown that vulnerability curves generated with centrifugation suffer from artifacts when applied to long-vesselled species (Cochard *et al.*, 2010; Choat *et al.*, 2010; McElrone *et al.*, 2012; Torres-Ruiz *et al.*, 2014). At the heart of this artifact is the issue of open vessels, which occur in stem samples when the maximum vessel length exceeds the sample size, leading to xylem vessels that are unobstructed by pit membranes from end-to-end or that only have a single pit membrane (open from sample end to the middle of the segment). Too many open vessels are thought to lead to anomalous 'r' shaped vulnerability curves that over-estimate vulnerability to cavitation (Choat *et al.*, 2010; Martin-StPaul *et al.*, 2014). A review of all available vulnerability data supports the conclusion that all centrifuge methods are prone to artifact when applied to long vesselled species (Cochard *et al.*, 2013).

Why would open vessels lead to anomalous 'r' shaped vulnerability curves? One hypothesized mechanism may be the role of microbubbles (Cochard *et al.*, 2005; Sperry *et al.*, 2012; Wang *et al.*, 2014), which we term the 'Champagne effect.' This Champagne effect may occur when any solution not previously filtered by an intervessel pit membrane is potentially contaminated with either microbubbles or dust motes that may serve as embolism nuclei (Sperry *et al.*, 2012; Rockwell *et al.*, 2014; Wang *et al.*, 2014). Two possible microbubble sources are 1) the solution in the centrifuge reservoirs or 2) the solution used to measure flow or flush samples (Sperry *et al.*, 2012; Rockwell *et al.*, 2014). Microbubbles can move in open vessels by buoyancy towards the center or axis of rotation in a spinning sample until either the pressure reaches a critical threshold, causing

them to expand and form artifactual emboli, or their movement is stopped by an end wall (Sperry *et al.*, 2012; Rockwell *et al.*, 2014; Zhang & Holbrook, 2014). While species with short vessel lengths would have intact vessels with pit membranes that can filter solution and impede the movement of microbubbles, microbubbles causing the Champagne effect would be magnified in samples with long vessels that would be cut open during sample preparation or in vessels that only have a single pit membrane. This was tested in one experiment by (Wang *et al.*, 2014), who spun stems at tensions too low to induce "real" cavitation (0.031MPa) for 4 hours and observed a decline in stem conductivity for a long-vesselled species, *Robinia pseudoacacia*, over time as artifactual cavitation occurred. This was likely caused by microbubbles moving towards the axis of rotation, where the greatest tension occurs.

To test the Champagne effect, we constructed vulnerability curves and native and flushed xylem water extraction curves for five species with varying vessel lengths. With water extraction curves, no solution is ever introduced to the sample and there is no flow in the sample, which effectively eliminates the microbubble – embolism nuclei effect. Instead, this method measures the water released by the sample at each pressure step, also known as capacitance (Meinzer *et al.*, 2003; Vergeynst *et al.*, 2014). Water stored in living cells and intercellular spaces is first released, followed by water released via cavitation. Comparing vulnerability curves to native extraction curves serves as a test for when "real" cavitation is actually occurring. If the early loss of conductance in "r" shaped vulnerability curves is not due to cavitation (or rather, if it is artifactual cavitation due to microbubbles), this is further evidence of the long vessel artifact and the Champagne

effect. We then compared native versus flushed xylem water extraction curves to test the effects of flushing on curve shape and different water storage phases. Flushing samples could introduce microbubbles and magnify the Champagne effect, altering water storage phases and water extraction curve shape. Accurately constructing vulnerability curves is essential to correctly characterizing xylem vulnerability to cavitation, and understanding the mechanisms underlying these potential artifacts can potentially lead to technique improvements and artifact solutions.

Methods

Study species

Experiments were performed on five different species with varying vessel lengths, from trachieds (a few mm) to vessels >1m in length, harvested on the campus of University of Bordeaux, Talence, France. Study species in order of increasing vessel length included *Pinus spp., Populus nigra*, *Fagus sylvatica*, *Prunus cerasifera*, and *Eucalyptus spp.*

Maximum vessel length

Maximum vessel length was determined using the air infiltration technique (Zimmermann & Jeje, 1981; Ewers & Fisher, 1989) by collecting long stem samples (>1m) and injecting compressed air into the basal end while the distal end is submerged in water. The distal end was cut under water in 5cm increments until air bubbles were observed, indicating open vessels. Hence, the remaining uncut shoot length constituted the maximum vessel length.

Xylem vulnerability curves

Vulnerability curves were constructed using the Cavitron technique (Cochard, 2002; Cochard *et al.*, 2005). Samples (~1m in length) were harvested and the leaves immediately removed before being brought back to the lab. Samples were immersed in water and cut to the corresponding length depending on which diameter rotor was to be used, with the sample ends cleanly cut with a fresh razor blade. Rotor diameters and therefore stem sample lengths included 14cm, 27cm, and 42cm. Around 3cm of bark were removed from each end of the stem samples to fit inside the cuvettes or reservoirs. Samples were placed in the rotor and spun at low speeds producing only moderately negative pressure to first measure the maximum stem conductivity (K_{max}) by injecting a 10mM KCl and 1mM $CaCl_2$ solution into the Cavitron that flowed through the stem. The rotational speed was then increased in a stepwise manner to measure percent loss of conductivity (PLC) as:

$$PLC = 100 \times (1-K/K_{max})$$

Curves were conducted until >90% PLC was reached or when the maximum rotational velocity for the Cavitron was achieved, whichever came first. In the 14cm rotor, the maximum water potential was −3.2MPa because the maximum rotational velocity of the rotor was 10000rpm. Vulnerability curves were constructed by plotting PLC versus xylem pressure and fitting a Weibull function using SAS to calculate P_{50}, the water potential at which 50% of conductivity is lost.

Xylem water extraction curves

Xylem water extraction curve sample collection and preparation was the same as for vulnerability curves (see above), but differed in that all bark was completely removed from the samples. In addition, we had two treatments for our water extraction curves: native and flushed (vacuum infiltrated). Native samples were not flushed and contained only native sap. Flushed stem samples were immersed in 10mM KCl and 1mM $CaCl_2$ solution (the same solution used to measure flow in vulnerability curves) and placed under house vacuum for >2 hours or until all native emboli were removed. Samples were then placed in the 27cm rotor with intact cuvette reservoirs. Samples were initially spun at -0.1MPa to visualize the menisci, after which the speed was increased in a stepwise fashion. Stems were spun at each pressure step until the menisci no longer moved and they overlapped, meaning no water was being released and that equilibrium was achieved (typically ~2min). This was repeated until water release became negligible or until the menisci became completely separated, indicating complete sample cavitation. Water extraction curves were calculated by first removing points between 0 and −0.8MPa to exclude elastic water storage (Tyree & Yang, 1990), then fitting a Weibull function to the remaining points using SAS to calculate P'_{50}, or the water potential at which 50% of xylem water was released. Additional native water extraction curves for *Pinus* and *Prunus* were measured using the 14cm rotor to test if water extraction curve shape may shift between 's' and 'r' shaped within a species. As the maximum rotational velocity for this rotor is only 10000rpm, the maximum water potential was −3.2MPa. As such, water extraction curves conducted using the 14cm rotor could not be run to full sample

cavitation and water release in order to calculate percent water extracted or P'_{50}. However, the difference in curve shape, as well as differences in water storage phases, are obvious by plotting the "raw" curves (absolute volume of water released at each pressure step).

Vessel anatomy

Four to five cross-sections were cut from each stem used for water extraction curves using a sliding microtome (GSL1 Microtome, Schenkung Dapples, Switzerland). Cross-sections were stained with safranin (1%), fixed on microscope slides and observed with a light microscope (DM2500, Leica, Germany). Photos of each section were taken with a digital camera (DFC290, Leica, Germany) interfaced with computer software (Leica QWin v.3). Images were analyzed with ImageJ (v.1.49h) to measure vessel lumen diameter and the percent of vessel lumen area, in order to calculate vessel lumen volume.

Results

Comparing vulnerability curves among three rotor sizes

Maximum vessel length varied between the five study species, from tracheids that are only a few mm long for the coniferous *Pinus* to vessels 50 to 100cm long for *Eucalyptus* (*Pinus*<*Populus*<*Fagus*<*Prunus*<*Eucalyptus*; Table 1). *Pinus*, *Populus*, and *Fagus* all had 's' shaped curves in all three rotor sizes, while *Eucalyptus*, which has extremely long vessels, had 'r' shaped curves in all three rotors (Figure 2). *Prunus*, which has an intermediate vessel length, displayed a shift in vulnerability curve shape, from an 'r'

shaped curve in the 14cm diameter rotor, where the maximum vessel length exceeded the sample length, to an 's' shaped curve in the 42cm diameter rotor, where the maximum vessel length was less than the sample length.

P_{50} varied between species, from -2.32 for *Populus* to -5.95 for *Prunus* (Table 2). For tracheid-bearing and short vesselled species that did not display any shift in vulnerability curve shape between rotor sizes, there was also no change in the P_{50} between rotor sizes, as seen with *Pinus*, *Populus*, and *Fagus*. However, when species had an intermediate vessel length and did display a shift in vulnerability curve shape between rotor sizes, they also displayed a change in P_{50} (Table 2). This is exemplified by *Prunus*, which had an 'r' shaped vulnerability curve and a more vulnerable P_{50} of -4.31MPa in the 14cm diameter rotor, but when a larger rotor was used the curves became 's' shaped and the P_{50} more resistant to -5.95MPa.

Comparing native water extraction curves to vulnerability curves

P'_{50} varied between -2.84 for *Populus* and -6.64 for *Prunus* (Table 2). P_{50} and P'_{50} were tightly correlated (Figure 5), but P'_{50} was always significantly more resistant than P_{50}. Native water extraction curves tended to be 's' shaped and displayed different phases of water storage, as proposed by (Tyree & Yang, 1990). As the later stage of water release is due to cavitation (Tyree & Yang, 1990; Vergeynst *et al.*, 2014) and this methodology is not subject to the Champagne effect, it is possible to compare native water extraction curves to vulnerability curves and determine when actual versus artificial cavitation is occurring in vulnerability curves. *Pinus* shifted to cavitation water release around -3MPa,

which is just prior to its P_{50} of -3.70MPa. *Populus* shifted to cavitation water release around -1.5MPa, which is just prior to its P_{50} of -2.31MPa. *Fagus* shifted around -3.0MPa, just prior to its -4.05MPa P_{50}. According to its native water extraction curves, *Prunus* did not experience significant cavitation until -5MPa, which is just prior to the P_{50} measured using the 27 and 42cm diameter rotors of -5.90 and -5.95MPa respectively, but is *after* the 14cm P_{50} of -4.31MPa. This suggests that the initial cavitation in the 14cm 'r' shaped vulnerability curve is anomalous and adds further discredit to the validity of 'r' shaped vulnerability curves.

Comparing native versus flushed water extraction curves

Overall, water extraction curves were highly repeatable (Figure 3). However, there was greater variability between replicates in flushed water extraction curves than native curves. There were shifts in the range of water storage phases between the native and flushed treatments, with flushed water extraction curves releasing much more water during the initial phase than the native curves. Manipulating the sample length for native water extraction curves for *Pinus* and *Prunus* led to no differences in water extraction curve shape or shift in the initial water storage phase (Figure 4); only the flushed treatment showed a curve shift. Vessel lumen diameter varied between 15.8 μm for *Pinus* and 62.7 μm for *Eucalyptus*, and vessel lumen volume did not correspond with total volume of water released for water extraction curves.

Discussion

We did not find any change in the shape of vulnerability curves between different rotor sizes for tracheid-bearing, short-vesselled, and long-vesselled species. Tracheid-bearing and short-vesselled species, including *Pinus*, *Populus*, and *Fagus*, had maximum vessel lengths shorter than the rotor size used and always produced 's' shaped vulnerability and had no change in P_{50} no matter the rotor diameter. This indicates the Cavitron technique is robust to measure resistance to cavitation in these tracheid-bearing and short-vesselled species. However, the case is the opposite for *Eucalyptus*, which always produced 'r' shaped curves as it also always had a maximum vessel length longer than the available rotor sizes. Indeed, as long-vesselled *Eucalyptus* always produced 'r' shaped vulnerability curves, its P_{50} cannot be considered a true reference value. Only with *Prunus*, which has an intermediate vessel length, did we find a change in the shape of the vulnerability curve between rotor sizes. In the 42cm diameter rotor, *Prunus* would have few or no open vessels, where it also produced an 's' shaped vulnerability curve and a more resistant P_{50}. In the 14cm diameter rotor, where it displayed an 'r' shaped vulnerability curve and more vulnerable P_{50}, *Prunus* would be subject to the open vessel artifact. Overall, these results support the findings of (Cochard *et al.*, 2010a), who also showed an increased incidence of 'r' shaped curves as maximum vessel size exceeds rotor diameter.

Xylem water extraction curves displayed different phases of water storage, as proposed by (Tyree & Yang, 1990), including the initial phase of water released from living cells and intercellular spaces and the later phase of water released via cavitation

(Vergeynst *et al.*, 2014). While the percent of water released in each phase and the shape of the water extraction curves were different between the native and flushed treatments, native water extraction curves tended to produce 's' shaped curves no matter the maximum vessel length. Furthermore, there was no shift in water extraction curve shape within a species between rotor sizes. For example, while there was a shift in the vulnerability curve shape from 's' in the 27cm rotor to 'r' in the 14cm rotor for *Prunus*, there was no shift in water extraction curve shape between these two rotor sizes for *Prunus*. These results indicate water extraction curves are not subject to an open vessel bias like vulnerability curves are. In addition, our tight correspondence between P_{50} and P'_{50} is consistent with previous studies (Beikircher *et al.*, 2010; Cochard *et al.*, 2010b). However, within a species P'_{50} was always significantly more resistant than P_{50}, providing evidence that water extraction curves are not a new way to determine vulnerability to cavitation.

As water extraction curves are constructed without measuring flow in stem samples and no solution is ever introduced to the sample (except with flushed treatments), the Champagne effect is effectively eliminated with this technique. Hence we can compare the water potential at which water released due to cavitation occurs in water extraction curves with vulnerability curves to determine if cavitation is real or artifactual, especially for 'r' shaped vulnerability curves. For *Pinus*, *Populus*, and *Fagus*, the shift from the initial water release phase to the later cavitation release phase in the water extraction curves occurs prior to the P_{50} from the vulnerability curve, indicating the loss of conductance observed in the vulnerability curve is "real." With *Prunus*, this was

true for the ‘s’ vulnerability curves constructed using the 27cm and 42cm diameter rotors. However, comparing the water extraction curve with the 14cm vulnerability curve for *Prunus*, the shift to cavitation water release occurred *after* the P_{50}. This indicates the early loss of conductance measured with the 14cm diameter rotor is artifactual and likely due to the Champagne effect.

In comparing native versus flushed water extraction curves, we saw a significant shift in curve shape and the range of water potentials where the different phases of stored water were released. This was especially true for *Pinus*, *Fagus*, and *Prunus*. Native water extraction curves were generally ‘s’ shaped, even for long vesselled species and independent of rotor size, while flushed curves were not. Yet, this does not reveal why flushing might diminish the quality of water extraction curve measurements. One possibility is flushing introduces microbubbles, causing the Champagne effect and resulting in altered cavitation water release. Another possibility is that flushing fills portions of the stem that are normally not filled with water and causes the entire stem to behave differently in terms of water release dynamics, especially in the initial phase. A third possibility is that depending of the perfusion solution, flushing could alter the osmotic potential of stem sap such that the balance of tension and osmotic potential are altered leading to changes in water potential gradients within the stem during measurement. Although the precise mechanism of how flushing influences water extraction curves is still unknown, collecting stems early in the morning when plant water status is at its highest is likely to produce the most reliable curves.

Our study confirmed that microbubbles play a role in artifacts associated with centrifuge-based vulnerability curves. While the Cavitron technique is robust to measure xylem resistance to cavitation in tracheid-bearing and short-vesselled species, when the maximum vessel length exceeds the sample length, the Champagne effect may induce artifactual cavitation. This was demonstrated by the comparison of vulnerability curves and water extraction curves, especially for *Prunus*, which has an intermediate vessel length. Flushing altered the water release phases of water extraction curves, and is not recommended. While native water extraction curve were highly repeatable, P'_{50} was always more resistant than P_{50}, indicating water extraction curves are not a viable alternative to vulnerability curves. There was no correlation between stem vessel lumen volume and the volume of water released. We did not compare native versus flushed vulnerability curves because previous studies have shown flushed vulnerability curves to have more vulnerable P_{50} (Choat *et al.*, 2010). Future water extraction curve tests may compare ring porous versus diffuse porous species.

References

Alder NN, Pockman WT, Sperry JS, Nuismer S. **1997**. Use of centrifugal force in the study of xylem cavitation. *Journal of Experimental Botany* **48**: 665–674.

Allen CD, Macalady AK, Chenchouni H, Bachelet D, McDowell NG, Vennetier M, Kitzberger T, Rigling A, Breshears DD, Hogg EHT, *et al.* 2010. A global overview of drought and heat-induced tree mortality reveals emerging climate change risks for forests. *Forest Ecology and Management* **259**: 660–684.

Beikircher B, Ameglio T, Cochard H, Mayr S. **2010**. Limitation of the Cavitron technique by conifer pit aspiration.

Brodribb TJ. **2009**. Xylem hydraulic physiology: The functional backbone of terrestrial plant productivity. *Plant Science* **177**: 245–251.

Choat B, Drayton WM, Brodersen CR, Matthews MA, Shackel KA, Wada H, McElrone AJ. **2010**. Measurement of vulnerability to water stress-induced cavitation in grapevine: a comparison of four techniques applied to a long-vesseled species. *Plant, Cell & Environment* **33**: 1502–1512.

Choat B, Jansen S, Brodribb TJ, Cochard H, Delzon S, Bhaskar R, Bucci SJ, Feild TS, Gleason SM, Hacke UG, *et al.* 2012. Global convergence in the vulnerability of forests to drought. *Nature* **491**: 752–755.

Cochard H. **2002**. A technique for measuring xylem hydraulic conductance under high negative pressures. *Plant, Cell & Environment* **25**: 815–819.

Cochard H, Damour G, Bodet C, Tharwat I, Poirier M, Améglio T. **2005**. Evaluation of a new centrifuge technique for rapid generation of xylem vulnerability curves. *Physiologia Plantarum* **124**: 410–418.

Cochard H, Herbette S, Barigah TS, Badel E, Ennajeh M, Vilagrosa A. **2010a**. Does sample length influence the shape of xylem embolism vulnerability curves? A test with the Cavitron spinning technique. *Plant, Cell & Environment* **33**: 1543–1552.

Cochard H, Herbette S, Hernández EI, Holtta T, Mencuccini M. **2010b**. The effects of sap ionic composition on xylem vulnerability to cavitation. *Journal of Experimental Botany* **61**: 275–285.

Ewers FW, Fisher JB. **1989**. Techniques for Measuring Vessel Lengths and Diameters in Stems of Woody Plants. *American Journal of Botany* **76**: 645.

IPCC. **2014**. *Climate Change 2014: Impacts, Adaptation, and Vulnerability. Part A: Global and Sectoral Aspects. Contributions of Working Group II to the Fifth Assessment Report of the Intergovernmental Panal on Climate Change.* (CB Field, V Barros, DJ Dokken, KJ Mach, MD Mastrandrea, TE Bilir, M Chatterjee, KL Ebi, YO Estrada, RC Genova, *et al.*, Eds.). Cambridge, UK: Cambridge University Press.

Rockwell FE, Wheeler JK, Holbrook NM. **2014**. Cavitation and Its Discontents: Opportunities for Resolving Current Controversies. *Plant Physiology*.

Santiago LS, Goldstein G, Meinzer FC, Fisher JB, Machado K, Woodruff DR, Jones TJ. **2004**. Leaf photosynthetic traits scale with hydraulic conductivity and wood density in Panamanian forest canopy trees. *Oecologia* **140**: 543–550.

Sperry JS, Christman MA, Torres-Ruiz JM, Taneda H, Smirth DD. **2012**. Vulnerability curves by centrifugation: is there an open vessel artifact, and are 'r' shaped curves necessarily invalid? *Plant, Cell & Environment* **35**: 601–610.

Tyree MT, Sperry JS. **1988**. Do woody plants operate near the point of catastrophic xylem dysfunction caused by dynamic water stress? : answers from a model. *Plant physiology* **88**: 574–580.

Tyree MT, Yang S. **1990**. Water-storage capacity of Thuja, Tsuga and Acer stems measured by dehydration isotherms. *Planta* **182**: 420–426.

Wang R, Zhang L, Zhang S, Cai J, Tyree MT. **2014**. Water relations of Robinia pseudoacacia L.: do vessels cavitate and refill diurnally or are R-shaped curves invalid in Robinia? *Plant, Cell & Environment* **37**: n/a–n/a.

Zhang Y-J, Holbrook NM. **2014**. The stability of xylem water under tension: a long, slow spin proves illuminating. *Plant, Cell & Environment*: n/a–n/a.

Zimmermann MH, Jeje A a. 1981. Vessel-length distribution in stems of some American woody plants. *Canadian Journal of Botany* **59**: 1882–1892.

Table 3.1. Range of maximum vessel lengths and replication, and mean vessel diameters ± SE and replication for five study species.

Species	**Maximum vessel length (n) cm**	**Mean vessel diameter ± SE (n) µm**
Pinus sp.	Tracheids	15.8 ± 0.188 (488)
Populus nigra	10 − 50 (14)	40.6 ± 0.670 (227)
Fagus sylvatica	20 − 30 (5)	28.4 ± 0.430 (330)
Prunus cerasifera	35 − 45 (5)	28.9 ± 0.377 (347)
Eucalyptus sp.	50 − 100 (5)	62.7 ± 0.687 (336)

Table 3.2. The water potential at which 50% of hydraulic conductivity is lost (P_{50}), determined from vulnerability curves using the 14cm, 27cm, and 42cm diameter rotors, and the water potential at which 50% of xylem water of released (P'_{50}) determined from native xylem water extraction curves using the 27cm diameter rotor, for five study species. Differences in P_{50} among rotor sizes within each species are indicated by dissimilar letters ($p<0.05$). P_{50} measured in the 14cm diameter rotor for *Pinus* and *Fagus* could not be determined as curves were not run to completion due to the maximum rotational velocity of the rotor.

Species	**14cm P_{50} ± SE (n) Mpa**	**27cm P_{50} ± SE (n) Mpa**	**42 cm P_{50} ± SE (n) Mpa**	**P'_{50} (n) Mpa**
Pinus sp.	--	-3.70 ± 0.06 (5)[a]	-3.50 ± 0.12 (5)[a]	-4.41 (5)
Populus nigra	-2.19 ± 0.10 (5)[a]	-2.32 ± 0.05 (9)[a]	-2.22 ± 0.10 (6)[a]	-2.84 (5)
Fagus sylvatica	--	-4.05 ± 0.05 (6)[a]	-4.01 ± 0.08 (5)[a]	-4.47 (5)
Prunus cerasifera	-4.31 ± 0.28 (10)[b]	-5.90 ± 0.06 (9)[a]	-5.95 ± 0.04 (6)[a]	-6.64 (5)
Eucalyptus sp.	-1.10 ± 0.13 (6)[a]	-3.29 ± 0.35 (6)[b]	-1.34 ± 0.24 (6)[a]	-4.60 (5)

*P_{50} for *Eucalyptus* cannot be considered a true reference value because of the large number of open vessels leading to 'r' shaped curves that overestimate vulnerability.

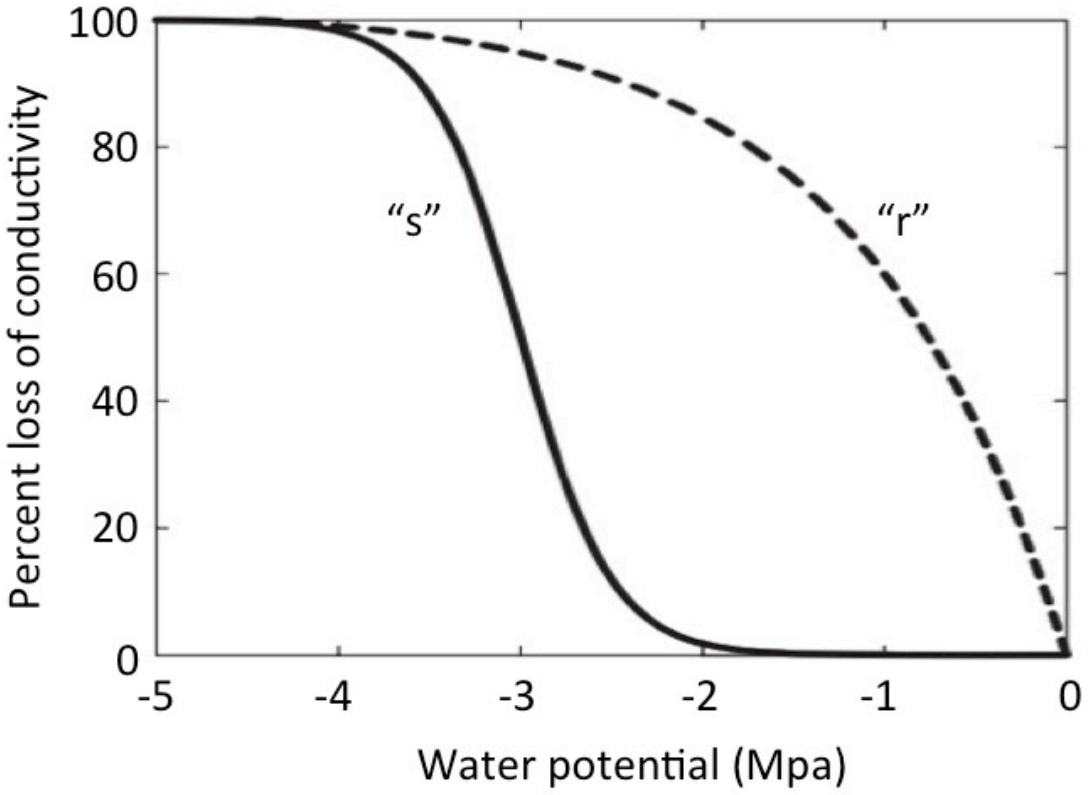

Figure 3.1. Representative vulnerability curves showing the change in percent loss of conductivity versus water potential for 's' shaped curves (solid line) and 'r' shaped curves (dashed line). 'r' shaped vulnerability curves are significantly more vulnerable to cavitation than 's' shaped curves. Redrawn from (Cochard *et al.*, 2010a).

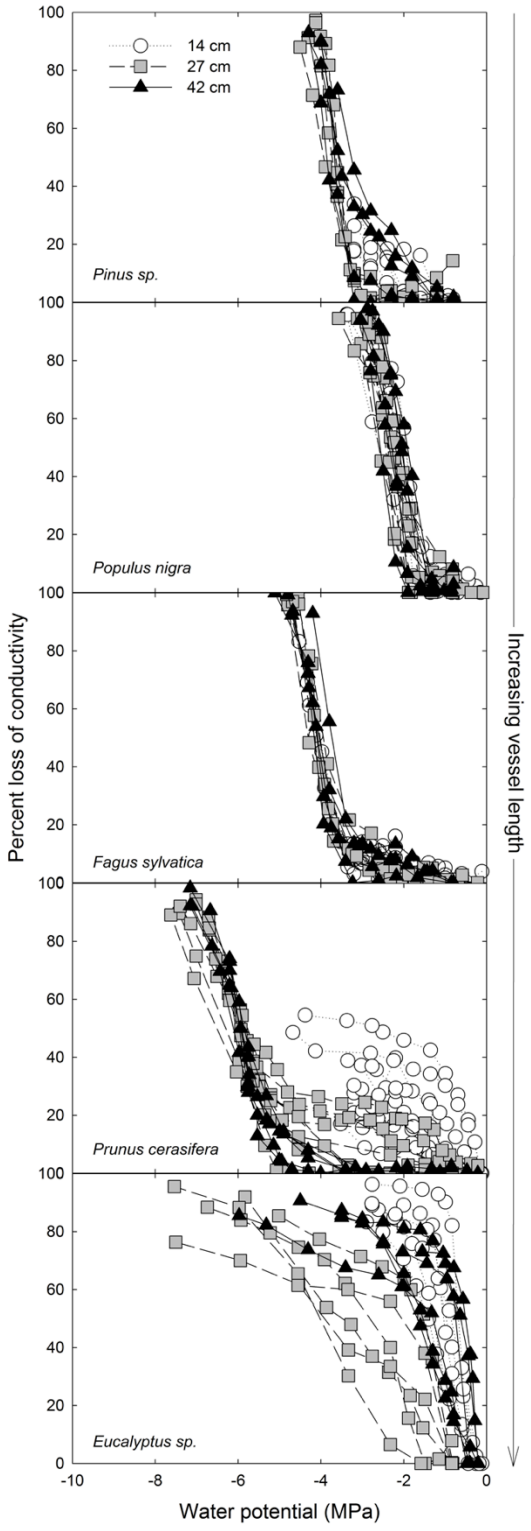
14 cm
27 cm
42 cm
Pinus sp.
Populus nigra
Fagus sylvatica
Prunus cerasifera
Eucalyptus sp.
Percent loss of conductivity
Water potential (MPa)
Increasing vessel length

Figure 3.2. Vulnerability curves constructed using the 14cm diameter (open circles), 27cm diameter (gray squares), and 42cm diameter (black triangles) rotors in the Cavitron for *Pinus sp.* (14cm n=5; 27cm n=5; 42cm n=5), *Populus nigra* (14cm n=5; 27cm n=9; 42cm n=6), *Fagus sylvatica* (14cm n=5; 27cm n=6; 42cm n=5), *Prunus cersifera* (14cm n=10; 27cm n=9; 42cm n=6), and *Eucalyptus sp* (14cm n=6; 27cm n=6; 42cm n=6).

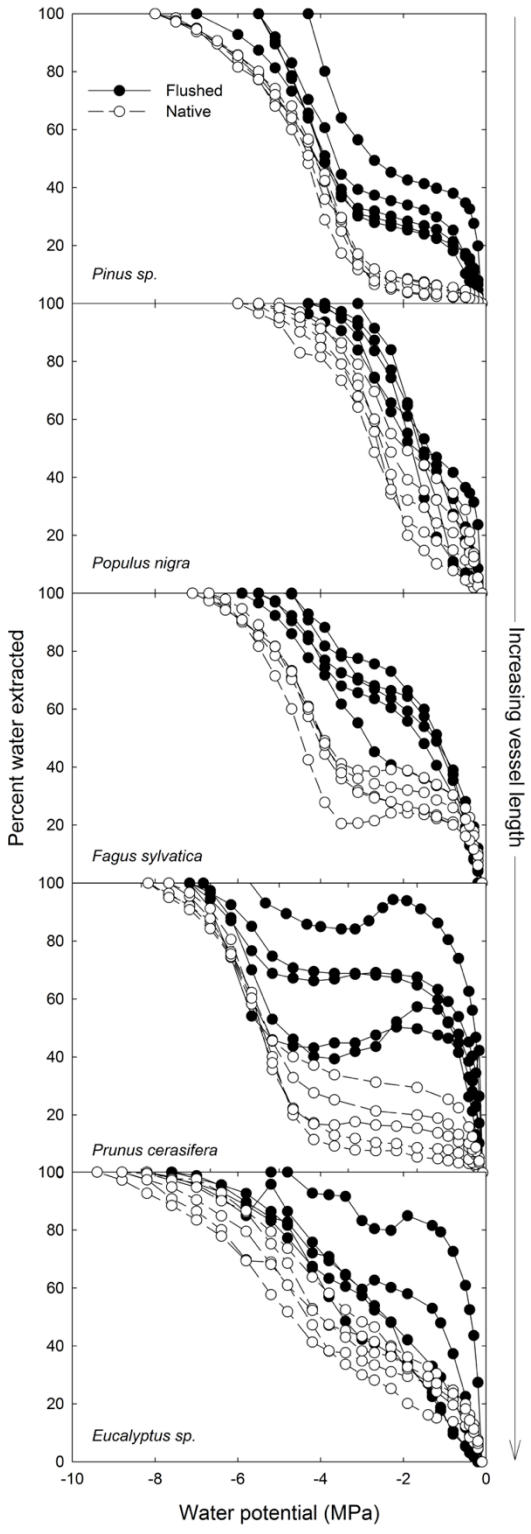
Flushed
Native
Pinus sp.
Populus nigra
Fagus sylvatica
Prunus cerasifera
Eucalyptus sp.
Percent water extracted
Water potential (MPa)
Increasing vessel length
100
80
60
40
20
0
-10
-8
-6
-4
-2
0

Figure 3.3. Xylem water extraction curves constructed using the 27cm diameter rotor in the Cavitron for native (open circles) and flushed (close circles) samples of *Pinus sp.*, *Populus nigra*, *Fagus sylvatica*, *Prunus cersifera*, and *Eucalyptus sp*., replicated five times for each species and each treatment.

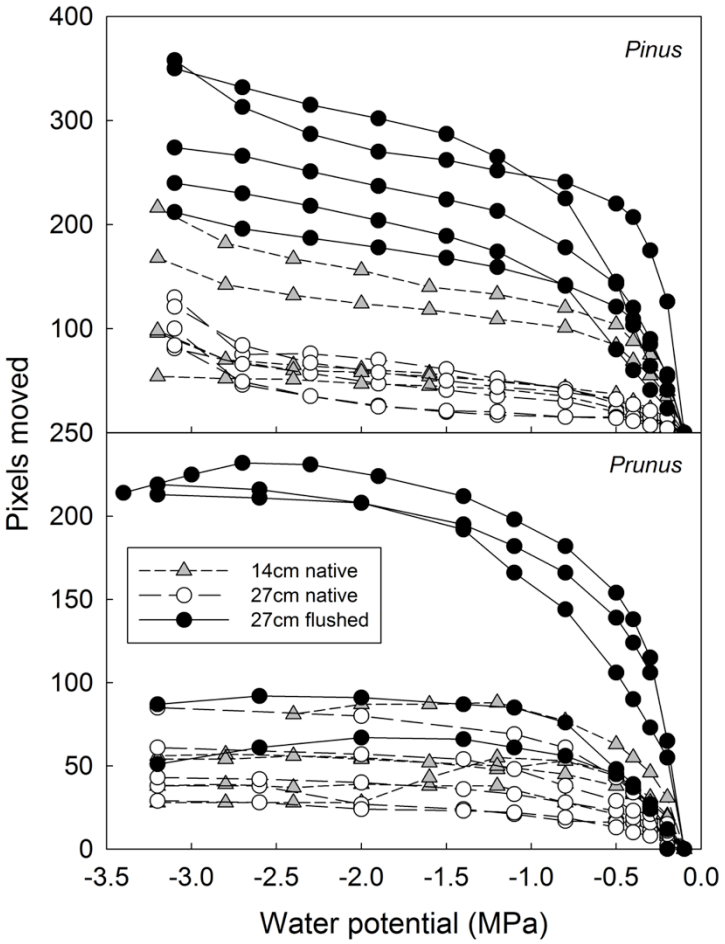

Figure 3.4. Xylem water extraction curves plotted as water potential versus number of pixels the menisci moved (a proxy for volume of water released) for *Pinus* and *Prunus* for 27cm long flushed samples, 27cm long native samples, and 14cm long native samples. As the maximum rotational velocity of the 14cm diameter rotor is 10000rpm, the maximum pressure was -3.2MPa. Hence, water extraction curves constructed with the 14cm rotor could not be run to full sample cavitation and water release, and percent water extracted could not be calculated.

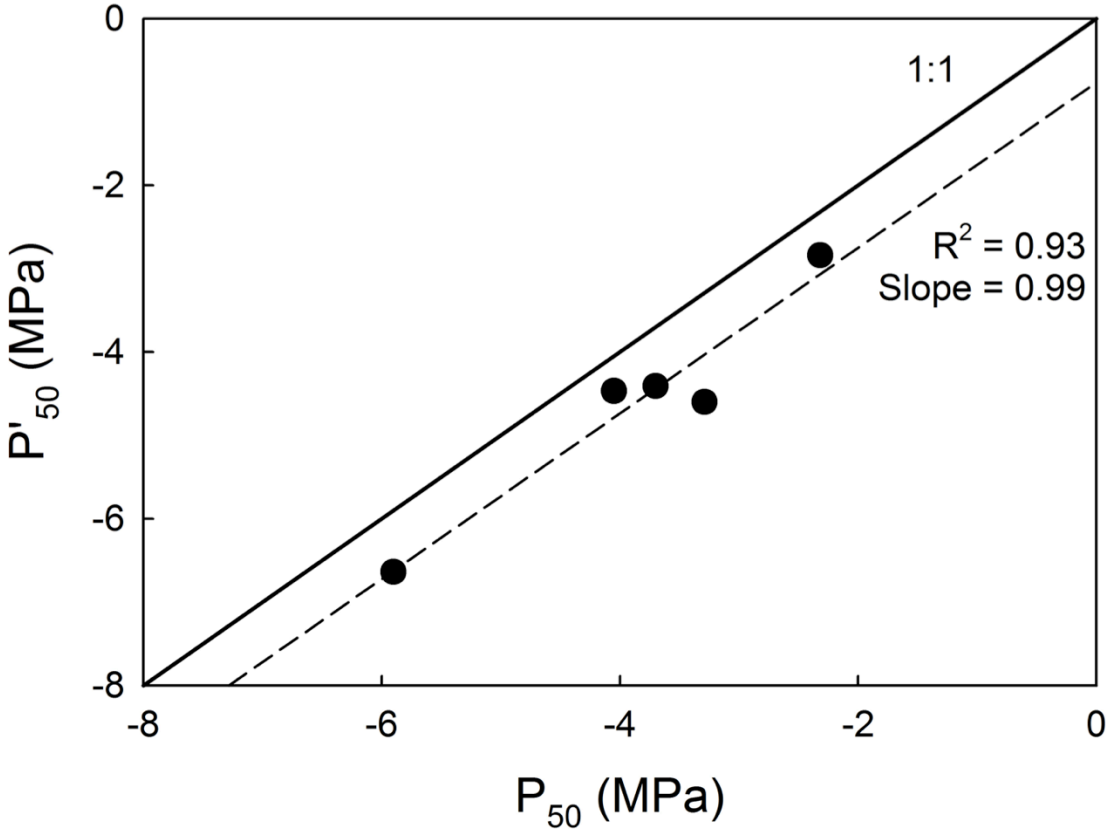

Figure 3.5. The water potential at which 50% of hydraulic conductivity is lost (P_{50}) as calculated from vulnerability curves versus the water potential at which 50% of xylem water was released (P'_{50}) as calculated from water extraction curves, both constructed using the 27cm diameter rotor in the Cavitron.

Conclusions

Overall, there are three major points to draw from this dissertation. The first is that even though species may co-occur and be subject to identical temperature and precipitation conditions, differences in traits between species facilitates resource partitioning and niche differentiation. These same differences, however, mean that some species are more susceptible to environmental change than others, illustrating a second conclusion. This was highly evident by the different hydraulic safety margins documented in Chapter 1, as well as the response of *Artemisia* to long-term nitrogen deposition, but the lack of response by *Adenostoma*, *Ceanothus*, and *Salvia* to increased nitrogen. Finally, the importance of accurate techniques for correctly quantifying plant drought adaptation traits is illustrated by the role of the Champagne effect in the open vessel artifact behind vulnerability curves.

Xylem vulnerability to cavitation and P_{50} were common to all three dissertation chapters. While there is currently a debate about whether or not the long vessel bias may also affect the static rotor as it does the Cavitron, the importance of this trait cannot be overstated. For example, (Choat *et al.*, 2012) shows that 70% of forest species worldwide operate very closely to the point of hydraulic failure. This means that while P_{50} may vary widely across species and climate types, even woody plants in wet forests may be vulnerable to drought mortality with climate change. This understanding is of particular importance in California, which has a seasonally and annually variable climate and may be a climate change hot spot (Diffenbaugh *et al*., 2008). Native species maybe unable to adapt to increased abiotic stress and be replaced by invasive competitors. Currently, only

15% of coastal sage scrub in intact (Castellanos & Mendoza 1991), making it an endangered ecosystem. Further threats may push this ecosystem to extinction.

There is a broad range of future studies that can expand this research. For example, the inclusion of additional vegetation types from other areas in California's Floristic Province will provide a broader understanding of how this state may impact by future environmental change. In addition, studying the effects of other types of environmental change will be beneficial. For example, California's Mediterranean-type climate is a highly fire-prone landscape. However, the increasing wildland-urban interface is leading to mostly human ignited fires. Changes in precipitation and fire regimes will have negative consequences for this biodiversity hotspot. Additionally, physiological data such as that presented here may go into models to predict how species and ecosystems may behave under altered conditions. Overall, studies such as this can also be expanded to applied research to inform management decisions and aid in the conservation of native landscapes.

References

Castellanos, A., and R. Mendoza. 1991. "Aspectos socioeconomicos." *La serva de la biosfera El Viscaino en la peninsula de Baja California Sur. Centro de Investigaciones de Baja California Sur, La Paz:* 33-52.

Choat B, Jansen S, Brodribb TJ, Cochard H, Delzon S, Bhaskar R, Bucci SJ, Feild TS, Gleason SM, Hacke UG, *et al.* 2012. Global convergence in the vulnerability of forests to drought. *Nature* **491**: 752–755.

Diffenbaugh NS, Giorgi F, Pal JS. **2008**. Climate change hotspots in the United States. **35**: L16709.